Environmental Setting for Reef Building in the Red Sea

2

James Churchill, Kristen Davis, Eyal Wurgaft, and Yonathan Shaked

Abstract

The Red Sea is a distinct marine system, which, due to its limited lateral extent, is strongly influenced by the surrounding arid and semiarid terrestrial environment. Among large marine bodies, it is unusually saline, owing to a high rate of evaporation relative to precipitation, and warm. The physical environment of the Red Sea has been subject to scientific research for more than a century, with considerable advances in understanding achieved in the past two decades. In this chapter, we review the current state of knowledge of the Red Sea's physical/chemical system. The bulk of the chapter deals with the marine environment. Attention is given to a variety of topics, including: tides and lower-frequency motions of the sea surface, circulation over a range of space and time scales, the surface wave field, and the distributions of water properties, nutrients, chlorophyll-*a* (chl-*a*) and light. We also review the current understanding of atmospheric conditions affecting the Red Sea, focusing on how atmospheric circulation patterns of various scales influence the exchange of momentum, heat, and mass at the surface of the Red Sea. A subsection is devoted to geology and reef morphology, with a focus on reef-building processes in the Red Sea. Finally, because reef building and health are tightly linked with carbonate chemistry, we review the Red Sea carbonate system, highlighting recent advances in the understanding of this system.

J. Churchill (✉)
Woods Hole Oceanographic Institution, Woods Hole, MA, USA
e-mail: jchurchill@whoi.edu

K. Davis
University of California, Irvine, Irvine, CA, USA

E. Wurgaft
Ben-Gurion University of the Negev, Beer-Sheva, Israel

Y. Shaked
Hebrew University of Jerusalem, Jerusalem, Israel

Keywords

Red Sea geology · Red Sea reef morphology · Atmospheric forcing · Basin-scale circulation · Mesoscale processes · Eddies · Surface waves · Carbonate system · Nutrient and light distribution

2.1 Geology and Reef Morphology

Like most reefs worldwide, modern reefs in the Red Sea were initiated during the Holocene (Braithwaite 1987). Rapid changes in sea level following the end of the last glacial maximum, ca. 18 ka, resulted in old reefs being abandoned and the initiation of new reefs at higher levels over what was previously sub-aerial substrates (Montaggioni 2000, 2005; Dullo 2005). During the Holocene, as rates of sea level rise declined, reefs developed into what we recognize today as large structures that often represent thousands of years of growth.

In the Red Sea and its northern tributaries, the Gulf of Suez and the Gulf of Aqaba, the effects of changing sea level were especially pronounced. The Red Sea is connected to the Gulf of Aden and the Indian Ocean through the narrow and shallow (137 m deep and 29 km wide) strait of Bab al Mandab. During glacial times, when sea level was more than 100 m lower than during interglacial periods, water exchange between the Red Sea and the Indian Ocean was very limited (Almogi-Labin et al. 1991; Arz et al. 2007; Biton et al. 2008). Limited water exchange coupled with little freshwater input from the surrounding arid lands and high evaporation rates, resulted in high salinity within the Red Sea during glacial periods (Morcos 1970; Felis et al. 2000). It has been estimated that Red Sea salinities during the last glacial maximum were 50 psu or greater (Siddall et al. 2003; Almogi-Labin et al. 2008; Biton et al. 2008; Legge et al. 2008), a level generally considered too high for coral growth (Kleypas et al. 1999).

In the Red Sea, temperature and salinity vary over latitude, with the northern end generally being cooler and more

saline (Biton et al. 2010). Coral reefs in the northern Red Sea and the Gulf of Aqaba are today among the northernmost reefs in the world. The worldwide reef distribution is thought to be limited primarily by temperature: coral reefs are not found in seas where the annual minimum temperature is lower than 18–20° (Kleypas et al. 1999; Schlager 2003). Sea surface temperature in the northern Red Sea during the last glacial maximum is estimated to have been 4 °C lower than today. It therefore seems unlikely that coral reefs were abundant in the northern Red Sea during glacial times. Whether no coral enclaves survived glacial periods within the Red Sea is debatable, but it seems that colonization of the present coastline by coral reefs most likely involved a south to north migration, rather than strictly a local reef rise coupled with the rising sea level (Kiflawi et al. 2006). Whatever the re-colonization pattern, fossil reefs in areas of tectonic uplift along the Red Sea coast indicate repeated establishment of reefs during interglacial times (Al-Rifaiy and Cherif 1988; Gvirtzman et al. 1992; Gvirtzman 1994; El-Asmar 1997).

The Red Sea may be viewed as an elongated, nearly land-locked, basin that is in the process of becoming an ocean (Bonatti 1985). Magmatism and sea floor spreading is occurring along the southern and central parts of the basin, but the northern basin is still being rifted (Joffe and Garfunkel 1987; Cochran and Martinez 1988; Bosworth et al. 2005). Along large portions of the coast, this young rifting process results in an often-steep topography of exposed crystalline basement rocks, punctuated by large alluvial fans transporting coarse erosion products from the highlands to the sea (Ben-Avraham et al. 1979; Bosworth et al. 2005). Sea level changes coupled with intense tectonic activity sometimes result in the drowning, exposure or burial of reefs (Shaked et al. 2004; Makovsky et al. 2008). This forces the establishment of younger reefs, displaying initial stages of development (Shaked et al. 2005).

The coastal plain in the area of the southern Red Sea is wider with gentler slopes than the coastal plain adjacent to the northern Red Sea (Bohannon 1986). Incision and alluvial transport in the area of the southern Red Sea were enhanced with the glacial-interglacial cycles of sea level fall and rise. Dropping sea level during glacial times lowered the base level and enhanced erosion and transport, whereas post-glacial sea level rise inundated the newly created alluvial fans and the crystalline hillsides. Since much of the area is arid, vegetation is scarce and the substrate available for coral settlement is mostly bare basement rock, conglomerates and poorly sorted alluvial fans of coarse material intercalated with fine sands and silts (Khalil and McClay 2009).

Coral reef morphology is greatly influenced by antecedent topography. A gradually sloping substrate will result in wider reefs, either as sea level rises and the reef retreats shoreward. When sea level is stable, the reef can easily expand seaward. The reefs formed over gently sloping topography are often separated from shore by a wide lagoon. The Red Sea with its generally steep slopes is characterized by fringing reefs, hugging the shoreline (Dullo and Montaggioni 1998). Exceptions occur where antecedent topography included hills and topographic highs lining the sea's margins. Following the post-glacial sea level rise, archipelagos and even barrier-type reefs were formed in such areas.

Corals tend to settle more easily, and coral reefs appear to develop more rapidly, on marine biogenic hard substrates (e.g., coralline algae or dead corals) (Harriott and Fisk 1987; Morse et al. 1996; Hoegh-Guldberg et al. 2007; Neo et al. 2009) than on crystalline rocks or loose substrates. Therefore, reefs may have taken longer to develop on steeply sloping crystalline margins than on gently sloping terraces of marine substrates. Reef growth along the margins is punctuated by active ephemeral river outlets and alluvial fans where loose unstable substrate inhibit coral settlement (Dullo and Montaggioni 1998). In the vicinity of such active fans, reef development seems to be slower than it is away from such features (Shaked et al. 2005). However, raised coral reefs along tectonically uplifting margins reveal repeated transgressional sequences, where sandy terrestrial sediments are overlaid by coarse beach sediments followed by fine lagoonal marine sediments and finally by coral reefs dated to previous interglacial periods (Al-Rifaiy and Cherif 1988; Gvirtzman 1994; Yehudai et al. 2017).

2.2   Atmospheric Setting

Because no point in the Red Sea is more than 150 km from land, a distance small compared to the scale of major weather systems, atmospheric conditions over the Red Sea are strongly influenced by the surrounding terrestrial environment.

For example, the atmospheric circulation over the Red Sea is appreciably affected by the coastal mountain chains running along the Red Sea margins. On a large-scale, these mountains tend to channel the air flow along the length of the Red Sea. This channeling is revealed by monthly-averaged winds, which tend to be aligned with the Red Sea's longitudinal axis (Patzert 1974; Sofianos and Johns 2001; Bower and Farrar 2015; Viswanadhapalli et al. 2017). The monthly-averaged winds also indicate a seasonal shift in the regional atmospheric regime associated with phases of the Arabian monsoon. Monthly-averaged winds of the summer period, roughly June–September, show an air flow directed to the southeast prevailing over the entire Red Sea. Monthly-averaged winds over the rest of the year reveal an air flow convergence, with winds directed to the southeast over the northern Red Sea and to the northwest over the southern Red Sea. In monthly-averaged wind fields, these opposing flows converge in the 18–20°N latitude range (Patzert 1974;
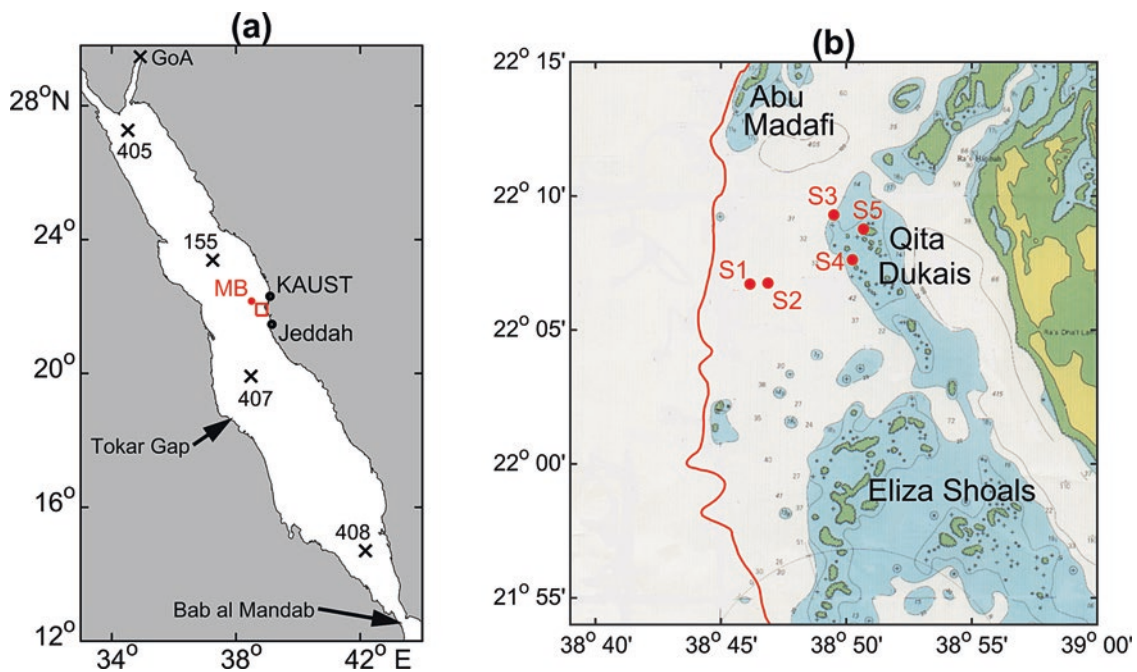
Fig. 2.1 Locations of measurements and features described in this chapter. (**a**) Large-scale map of the Red Sea showing the location of the meteorological buoy (MB) from which wind, wave and heat flux measurements were derived. Also shown are biogeochemical sampling stations (x's). Stations 405, 407 and 408 were sampled by the Geochemical Ocean Sections Study (GEOSECS) program in December 1977 (Weiss et al. 1983). Station 155 was sampled during the Mer Rouge (MEROU) program in 1982 (Papuad and Poisson 1986). Data from the northern Gulf of Aqaba (GOA) were sampled in 2011–2 as described by Wurgaft et al. (2016). (**b**) Locations of moored ADCPs (S1-S5), superimposed on a bathymetric map (United Kingdom Hydrographic Office) of the area outlined by the box in (**a**). Each ADCP was programmed to acquire data from which spectra of surface gravity waves could be computed. The red line traces the 100-m isobath, marking the eastern edge of the Red Sea basin. The buoy and ADCP were deployed as part of a collaborative field study involving Woods Hole Oceanographic Institution and King Abdullah University of Science and Technology

Sofianos and Johns 2001). However, wind data from a meteorological buoy deployed at 22° 10′ N (at "MB" in Fig. 2.1a), as part of a WHOI-KAUST cooperative investigation of the Red Sea, show that the northeastward air flow of the southern zone frequently extends well past the latitude limit suggested by the monthly-averaged winds. Although along-axis winds measured by the buoy are predominately directed to the southeast, episodes of northwestward wind frequently occur. Fifteen such events are seen in the 1-year record displayed here (Fig. 2.2).

Steering of atmospheric flow by the coastal mountains surrounding the Red Sea also produces intense winds directed across the Red Sea axis. These emerge from, or are directed into, mountain gaps. Of particular prominence are winds channeled through the Tokar Gap (Fig. 2.1a). During summer, strong eastward winds are funneled through the Gap and emerge onto the Red Sea (Jiang et al. 2009; Davis et al. 2015; Langodan et al. 2017a). In atmospheric models, these winds occur almost daily from mid-June to mid-September and are modulated diurnally, typically reaching a maximum strength, of up to 26 m s^{-1} (Davis et al. 2015), over 0700–0900 local (Saudi Arabian) time. When the Tokar Gap wind jet is most intense, large areas of the southern Red Sea are subject to strong eastward winds. As indicated by the model results of Jiang et al. (2009), the proportion of Red Sea surface area south of 20°N that experiences eastward winds of >10 m s^{-1} often exceeds 20% during July and August. During winter, air flow through the Tokar gap tends to be directed westward, resulting in funneling of air currents from the southern Red Sea into the Gap (Jiang et al. 2009).

Mountain-gap winds, emerging from the Arabian subcontinent are common phenomena over the northern Red Sea during winter (November – March) (Jiang et al. 2009; Bower and Farrar 2015). These westward wind jets occur at intervals of 10–20 days (see Fig. 2.2). They can persist for a number of days, though with diurnal modulation, and can encompass a large fraction, 10–40%, of the Red Sea area north of 20°N (Jiang et al. 2009).

Mountain-gap winds directed into the Red Sea carry many constituents of terrestrial origin into the marine environment. Prominent among these is dust. The Red Sea is situated in the Middle Eastern and North African 'dust belt' (0–40°N and 15°W–60°E). Roughly half the global dust emissions originate from this area (Prospero et al. 2002). Satellite imagery frequently show dust plumes originating at the major mountain gaps and extending across the Red Sea (Hickey and Goudie 2007; Jiang et al. 2009; Bower and Farrar 2015). Prakash et al. (2015) estimate that the Red Sea
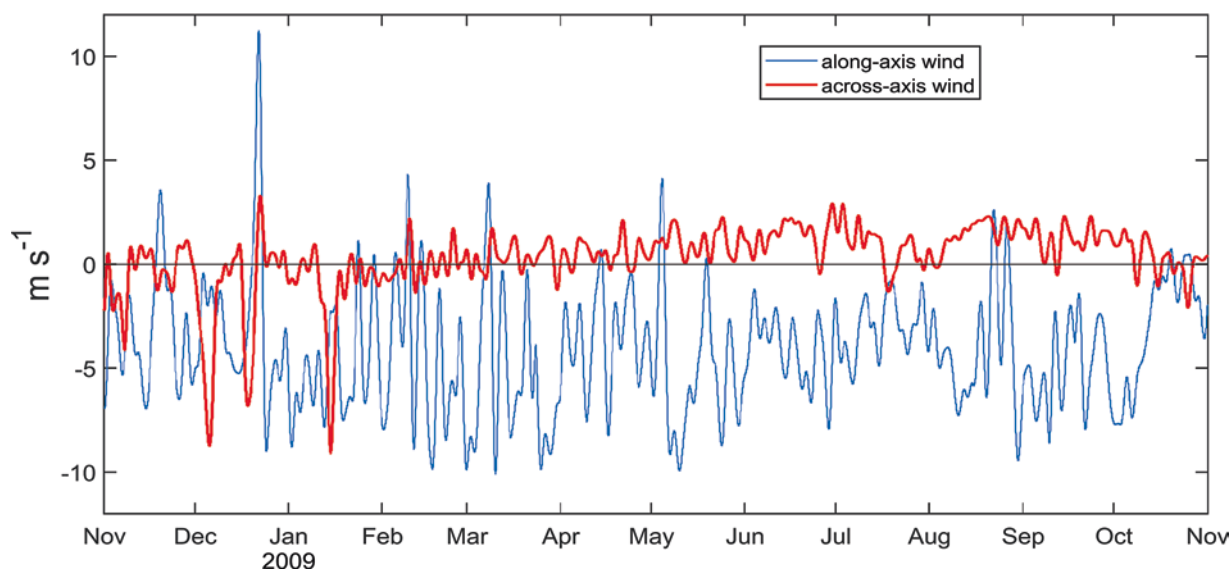
Fig. 2.2 A one-year record of low-passed filtered (66-h half-power point) along-axis (positive directed to the SSE) and across-axis (positive to the ENE) wind measured at meteorological buoy MB (Fig. 2.1a). The along-axis wind record shows the predominance of SSEward winds in the northern Red Sea, but also reveals a number of episodes of wind reversal to the NNWward direction associated with a northward extension of winter monsoon winds in the southern Red Sea. The across-axis wind record shows 'mountain-gap wind' events of strong WSWward winds (over Nov 2008 to Jan 2009) blowing across the Red Sea

experiences 5–6 significant dust storms per year, which may deposit as much as 6 Mt of solids into the Red Sea. The impact of dust deposition on the nutrient balance and productivity of the Red Sea may be significant, but has not yet been examined.

In addition to the mountain-gap winds, diurnally-modulated sea breezes, not necessarily associated with mountain-gap airflow, may be prevalent over the Red Sea during all seasons. Analysis of wind data from the WHOI-KAUST meteorological buoy (Fig. 2.1a) reveals a regularly occurring sea breeze in the central Red Sea that accounts for approximately 25% of the overall wind-stress variance (Churchill et al. 2014b). The observed sea breeze is highly polarized, with the major axis directed across-shore. The averaged (as a function of time of day) wind stress along the major axis is always directed onshore and exhibits a four-fold variation over the course of the day, reaching a maximum at 1700 local time (Churchill et al. 2014b).

While the surface wind stress can drive short-term currents and possibly basin-scale eddies (both of which are dealt with in the Marine Environment section below), model results indicate that the large-scale mean circulation of the Red Sea may be primarily the product of buoyancy loss associated with surface heat flux and evaporation (Sofianos and Johns 2002 and 2003).

It has long recognized that the rate of evaporation from the Red Sea far exceeds fresh water influx due to precipitation and runoff (Sofianos et al. 2002; and references therein). Estimates of the annual rate of evaporation from the Red Sea (computed from application of bulk formula to field data or from balancing the fresh water flux through the strait of Bab al Mandab with volume flux over the Red Sea surface) span a range 1.50–2.66 m year^{-1} (Table 1 of Sofianos et al. 2002). What may be the most tightly constrained estimate of the annual evaporation rate, based on moored measurements of currents and salinity through Bab al Mandab, is 2.06 ± 0.22 m year^{-1} (Sofianos et al. 2002). As indicated by analysis of data from the WHOI-KAUST meteorological buoy (Fig. 2.1), the evaporation rate varies seasonally about the mean, averaging roughly 3 m year^{-1} during winter and 1 m year^{-1} during summer (Bower and Farrar 2015). It also fluctuates on much shorter time scales. Bower and Farrar (2015) show that enhanced evaporation rates, exceeding 4.5 m year^{-1}, occur during the passage of cool and dry air carried past the mooring by the mountain gap wind events described above.

The net heat flux across the surface of the Red Sea also shows seasonal and shorter-term variations. The seasonal signal of net heat flux is characterized by net heat loss (transfer to the atmosphere) during winter months, roughly October–March, and net heat gain throughout the rest of the year (Ahmad et al. 1989; Tragou et al. 1999; Churchill et al. 2014b; Bower and Farrar 2015). Variations of the latent heat flux (associated with evaporation) and the incoming short-wave radiation are principally responsible for this seasonal net heat flux signal (Tragou et al. 1999; Bower and Farrar 2015). As documented by Papadopoulos et al. (2013) and Bower and Farrar (2015), the most intense events of winter-time heat loss over the northern Red Sea are associated with the westward passage of air from the Arabian subcontinent.

Papadopoulos et al. show that these events tend to correspond with a high pressure cell extending across the Mediterranean to central Asia.

The attenuation of incoming shortwave radiation due to dust may significantly contribute to the intense surface heat loss. Modeling results indicate that dust plumes over the Red Sea can extend vertically over 2–3 km and reduce the incoming shortwave, relative to clear-sky values, by up to 100 W m^{-2} (Kalenderski et al. 2013; Brindley et al. 2015; Prakash et al. 2015; Kalenderski and Stenchikov 2016). Based on results from a long-term (17 year) model simulation, Osipov and Stenchikov (2018) find that the overall impact of atmospheric dust is to cool the Red Sea surface, reduce the surface wind speed, and weaken both the water mass exchange through Bab-el-Mandeb and the overturning circulation.

Typically, the largest fluctuation of net heat flux occurs at a daily frequency, principally due to the day-night variation in incoming shortwave radiation (Figure 5 of Bower and Farrar 2015). Churchill et al. (2014b) demonstrate that the daily variation in net heat flux can lead to daily modifications in near-surface stratification (i.e. the formation of diurnal mixed layers) during periods of relatively weak surface wind stress. The warm surface layers observed by Churchill et al. form during the daylight hours of net heat gain and extend to between 5 and 20 m depths. They disappear during the nighttime hours of net heat loss, presumably due to convective vertical mixing initiated by the surface cooling.

As shown by Tragou et al. (1999), the yearly-averaged net heat flux varies spatially over the length of the Red Sea, with net heat loss north of roughly 18°N and net heat gain further south. According to calculations of Tragou et al., this spatial variation in net heat flux is the principal cause for a similar variation in net buoyancy flux, with a net buoyancy loss (gain) in the northern (southern) Red Sea.

2.3 Marine Environment

2.3.1 Basin-Scale Circulation

The geometry of the Red Sea, with an elongated basin and shallow sill at the Strait of Bab al Mandab (Fig. 2.1), combined with north-to-south gradients in surface heat flux and evaporation, result in meridional overturning and an exchange flow between the Red Sea and the Gulf of Aden. In a classic work, Phillips (1966) found similarity solutions for convectively driven flow forced by a uniform surface buoyancy flux that agree qualitatively with early observational studies of Red Sea circulation and water properties (Neumann and McGill 1962). The early summer observations by Neumann and McGill (1962) show a surface layer of warm (~30 °C) and relatively fresh (~36.5 psu) water, known as

Red Sea Surface Water (RSSW), flowing into the Red Sea through the Strait of Bab al Mandab (Fig. 2.1). As it flows north, this water cools and becomes more saline due to evaporation. The result is a gradual increase in density, causing the RSSW to sink in the northern Red Sea. It returns southward in a subsurface current of colder (~26 °C), more saline (~40–40.5 psu) water known as the Red Sea Outflow Water (RSOW).

The exchange of water through the Strait of Bab al Mandab changes seasonally in response to large-scale variations in buoyancy and wind forcing (Yao et al. 2014a, b). The two-layer, inverse-estuary type circulation observed by Neumann and McGill (1962) is strongest from October to May, with an average transport of RSOW water between the Red Sea and Gulf of Aden of 0.37 Sv (Sofianos et al. 2002). During summer (June to September), a three-layer exchange flow is observed through Bab al Mandab, with a mid-level influx of relatively cool and fresh Gulf of Aden water, known as Gulf of Aden Intermediate Water (GAIW), sandwiched between outward flowing layers of RSSW above and RSOW below (Murray and Johns 1997).

The relative importance of thermohaline and wind forcing in driving basin-scale circulation within the Red Sea has long been a topic of debate (e.g., Phillips 1966; Patzert 1974; Tragou and Garrett 1997). Seasonally varying winds are thought to modify the buoyancy-driven circulation – enhancing the surface inflow through the Strait of Bab al Mandab during the winter and inducing upwelling in the Gulf of Aden in the summer, resulting in the subsurface intrusion of GAIW described above. Three-dimensional numerical simulations of Red Sea circulation by Sofianos and Johns (2002, 2003), in which wind and buoyancy forcing are applied in isolation, reveal that buoyancy forcing is dominant in driving the overall circulation patterns and exchange through the Strait of Bab al Mandab. In their simulations, stronger evaporation in the northern Red Sea drives higher buoyancy fluxes and the formation of dense RSOW. The north-south gradient in buoyancy forcing results in a downward sloping sea surface to the north.

More recent simulations conducted by Yao et al. (2014a, b) with a highly realistic numerical model reveal a strong seasonality of the overturning circulation in the Red Sea. Their results show that the convectively-driven formation of RSOW in the northern Red Sea occurs principally over October–March and largely confined to the region north of 24°N. In the model-generated climatological fields (with the impact of basin eddies averaged out), the sinking of newly-formed RSOW takes place in a narrow downwelling-band at the eastern basin margin. In the model results, the newly formed GSOW is initially transported to the southeast in ~100–300 m deep boundary currents on the eastern and western basin margins. Yao et al. (2014b) show that basin-scale eddies (described below) can appreciably alter the

overturning flow structure, in a manner consistent with previous investigations (Maillard and Soliman 1986; Sofianos and Johns 2007). The modeled overturning circulation of the summer months (June–September) is dominated by the mid-level intrusion of GAIW, which is transported northward through the southern Red Sea in a eastern boundary current in the model results of Yao et al. (2014b), a result consistent with the observations of Churchill et al. (2014a).

2.3.2   Mesoscale Processes – Basin Eddies

The prevalence of eddies in the Red Sea basin has long been recognized (Quadfasel and Baudner 1993). Evidence of eddies within the basin has appeared in hydrographic survey data (Quadfasel and Baudner 1993), ADCP measurements (Sofianos and Johns 2007; Zhai and Bower 2013; Chen et al. 2014; Zarokanellos et al. 2017b), trajectories of satellite-tracked drifters (Chen et al. 2014) and numerical model results (Clifford et al. 1997; Sofianos and Johns 2003; Zhai and Bower 2013; Chen et al. 2014; Yao et al. 2014a, b). Eddies have been observed extending over diameters of order 200 km (Quadfasel and Baudner 1993), reaching depths of order 150 m (Sofianos and Johns 2007; Zhai and Bower 2013) and containing maximum velocities of ~ 1 m s^{-1} (Sofianos and Johns 2007).

A variety of statistical properties of Red Sea eddies has recently been determined from analysis satellite-altimeter-derived sea level anomaly (SLA) data acquired over 1992–2012 (Zhan et al. 2014). The results indicate that although eddies are formed during all seasons and over the full extent of the Red Sea, they are not uniformly distributed in space and time. Eddies appear with greatest frequency during the spring and summer (April–September) and in the central Red Sea (18–24°N), where the probability of a given point being within an eddy is close to 100%. Eddy diameter is also shown to vary spatially. Average eddy diameter is ~160 km in the northern and southern extremes of the Red Sea and is ~200 km in the central Red Sea. Zhan et al. (2014) note that this trend in diameter matches the variation in basin width and may indicate that eddy scale is limited by basin size. They also note that the limited zonal extent of the Red Sea may limit eddy lifetime, as eddies typically propagate zonally (westward in the northern hemisphere) which will would lead to significant coastal interaction and enhanced frictional dissipation. According to their analysis, Red Sea eddies have a mean lifetime of 45 days, with 95% the eddies expiring within 16 weeks.

A number of mechanisms for generating Red Sea eddies have been proposed. These include: baroclinic instability of flow with large vertical shear (Zhan et al. 2014), flow adjustment to seasonally varying buoyancy forcing (evaporation and heating) (Chen et al. 2014), and small-scale variations in the surface wind stress (Clifford et al. 1997; Zhai and Bower 2013). As opposed to the first two mechanisms listed above, the third may be highly localized. From analysis of satellite-derived (QuikSCAT) winds and SLA fields, Zhai and Bower (2013) link the formation of a dipole eddy pair (cyclonic and anticyclonic circulation cells) in the southern Red Sea with the summertime Tokar Gap wind jet. Their result is consistent with the model simulations of Clifford et al. (1997) in which the inclusion of forcing by orographically steered winds significantly increases the eddy prevalence in the modeled flow field. Because mountain gap winds over the Red Sea vary seasonally, they would produce a seasonally varying contribution to the overall eddy field.

Due to their prevalence and scale, which often spans the width of the Red Sea basin, eddies undoubtedly have a significant impact on coastal and basin ecosystems of the Red Sea. Acker et al. (2008) and Raitsos et al. (2013) offer evidence that basin-scale eddies transfer nutrients and/or chl-*a* from productive coastal reef regions to the oligotrophic waters of the Red Sea basin. Both set of investigators postulate that this phenomenon may be part of a 'mutual feedback mechanism' between coral reefs and the open basin, in which the seaward transport of nutrients stimulates blooms of phytoplankton in the deep basin, a fraction of which is transported back to the coastal reef region. The analysis of Churchill et al. (2014b) suggests that eddies may also be important in transporting mass and momentum from the deep basin to the coastal zone. They argue that the strongest currents observed in a coastal region of the central Red Sea may have been due to an along-shore pressure gradient arising from eddy-induced mass exchange between the deep basin and the coastal ocean.

A potentially important process that has yet to be extensively studied in the Red Sea is the enhancement of local productivity by mesoscale eddies. A number of investigators have found that mesoscale eddies in oceanic regions can promote productivity through vertical nutrient flux associated with changes in density structure linked with eddy generation and decay (e.g., Falkowski et al. 1991; Oschlies and Garçon 1998; McGillicuddy et al. 2007). For example, the upward doming of isopycnals that occurs within a cyclonic eddy in the northern hemisphere can deliver nutrient-rich deep water (typically found below the pycnocline) into the euphotic zone.

To our knowledge, in situ evidence of such a process is thus far limited to a study by Zarokanellos et al. (2017a). From data acquired within a cyclonic/anticyclonic eddy pair in the central Red Sea, they report a 50-m vertical isopycnal displacement associated with upward doming of isopycnals in the cyclonic eddy, and note the presence of relatively low oxygen concentrations (indicative of higher nutrient concentrations) in the surface mixed layer above the center of the cyclonic eddy.

2.3.3 Wind-Driven Flow

Wind fields over the Red Sea vary on seasonal, synoptic, and diurnal timescales as described above (Atmospheric Setting). While the basin-scale circulation patterns are dominated by seasonal buoyancy forcing, wind forcing also plays an important role by enhancing near-surface flows through the Strait of Bab al Mandab in winter and driving upwelled Gulf of Aden water into the Red Sea in summer (Basin-scale Circulation). Within the Red Sea basin, winds modify sea surface height on seasonal and synoptic (3–25 day) time scales (Sea Level Motions) and shape surface wave fields (Surface Waves). Cross-basin wind jets, or "mountain gap winds", impose a three-dimensionality on the essentially two-dimensional basin-scale thermohaline circulation, creating vorticity in near surface flows to form eddies (Mesoscale Processes – Basin Eddies) and coastal boundary layer currents (Bowers and Farrar 2015).

One aspect of wind-driven flow of particular importance to reef environments is upwelling/downwelling. The vertical movement of water associated with wind-driven upwelling has the potential to deliver deep, relatively cool and nutrient-rich water into the coastal reef regions. Statistical analysis applied by Churchill et al. (2014b) to water velocity and wind data acquired over 2008–2010 in the central Red Sea show a clear signal of wind-driven upwelling/downwelling in the Red Sea coastal zone. The signal is marked by an along-shore flow that is accelerated in the down-wind direction (positive wind stress/current correlation) and an across-shore flow that is directed to the right of the along-shore wind near the surface and to the left of the wind near the bottom.

To more fully demonstrate the effect of wind-driven upwelling/downwelling on the coastal temperature and velocity fields, we consider here (Fig. 2.3) temperature, velocity and wind stress data collected over 2008–2009 in the central Red Sea region (at site S2 in Fig. 2.1). The temperature records show periods of cooling water temperatures, of 1–3 weeks duration, superimposed on the annual temperature variation (Fig. 2.3a). The upwelling/downwelling signal observed by Churchill et al. (2014b) is apparent in the 2008–2009 current and wind stress data. Upwelling-favorable wind stresses (positive in Fig. 2.3b) are associated with offshore currents (positive "cross-wind currents"), which extend through most of the water column in the weakly stratified winter conditions and are concentrated in the upper mixed layer in summer and late spring when stratification is stronger (Fig. 2.3c). Southeast (along-shore) wind stress and near-
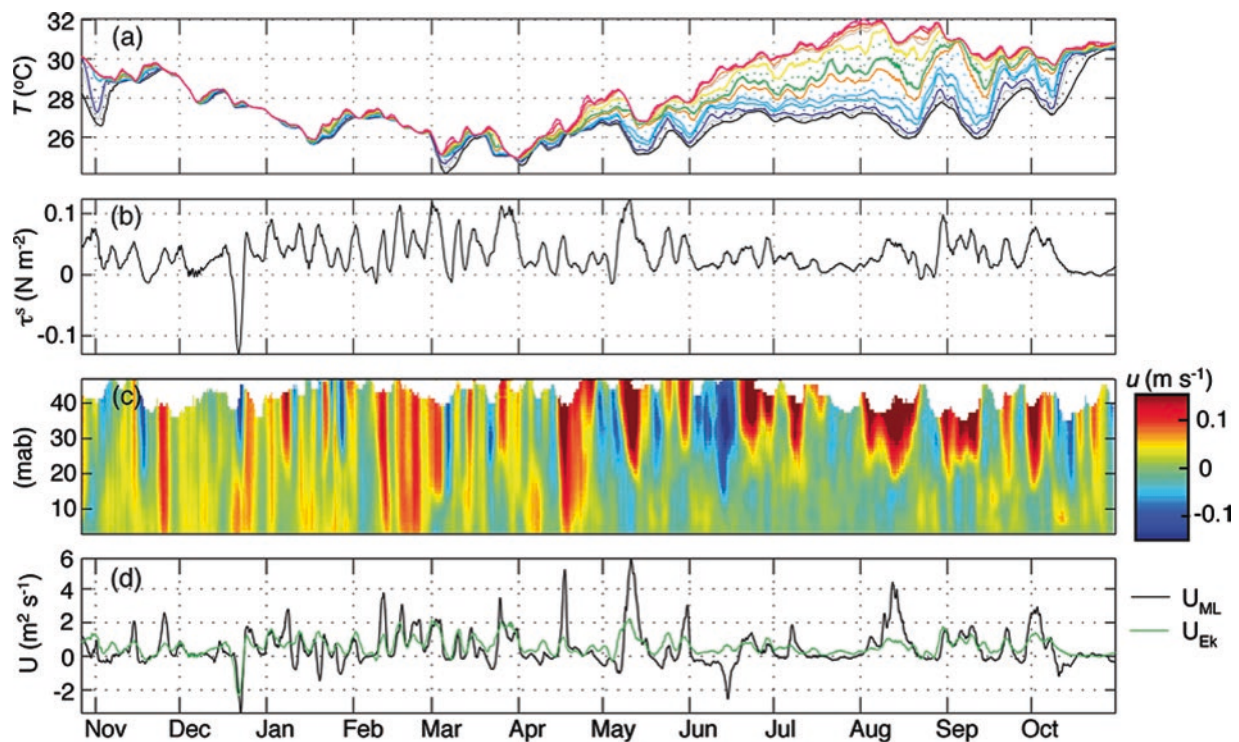

Fig. 2.3 2008–2009 time series of (**a**) water temperature at Mooring S1 (Fig. 2.1b) throughout the water column with warm colors (red/orange) near the surface and blues/black towards the bottom, (**b**) wind stress at meteorological buoy, rotated to 150°, approximately along-shore, (**c**) cross-wind currents at Mooring S2, positive towards 240°, approximately offshore, and (**d**) a comparison of upper mixed layer (U_{ML}) and Ekman (U_{Ek}) transports. In (**c**), (mab) represents meters above the bed. All time series shown were produced by filtering the original data with a low-pass filter with a 50-hr half-power point

surface cross-wind currents at S2 are significantly correlated over the entire year (r = 0.45 with 60 degrees of freedom (dof)), with a higher correlation over the time when the water is stratified (April–September; r = 0.6 with 30 dof). Churchill et al. show similar correlations.

The injection of wind energy into the upper ocean drives mixing, which can result in weak temperature gradients near the surface. The depth of the upper mixed layer, h_{ML}, calculated as the depth over which temperature is within 0.05 °C of the temperature at the top-most sensor (0.6-m depth) on the S2 mooring, varies appreciably, ranging from 3 m in summer to the full depth of the water column in winter. The cross-wind transport in the upper mixed layer, U_{ML} (estimated as the integral of the cross-wind component of the velocity from h_{ML} to the surface), compares well with Ekman transport computed from the wind stress, $U_{EK} = \dfrac{\tau^s}{\rho_0 f}$ (where τ^s, ρ_0 and f are the along-shore component of the surface wind stress, the upper layer water density and the Coriolis parameter, respectively). U_{Ek} and U_{ML} are correlated with a linear regression slope of 1.1 and r = 0.60, suggesting that cross-shelf transport is partially due to Ekman transport (Fig. 2.3d). However, as noted by Churchill et al. (2014b) the wind-driven upwelling/downwelling signal accounts for less than half of the overall variance of the sub-inertial (periods >2 days) flow observed at the central Red Sea mooring site. They observe significant departures of the observed transport from Ekman theory, indicating that other processes such as mesoscale eddies and coastal boundary currents may be important (see notable examples in mid-June and mid-August in Fig. 2.3d).

2.3.4 Sea Level Motions

Variations of the Red Sea water level span a range of order 1 m (Sultan et al. 1995a). Though relatively modest, these changes in the surface elevation may critically impact shallow ecosystems of the Red Sea. The crests of platform reefs, which are prevalent in the Red Sea and typically extend to depths of 1–2 m (DeVantier et al. 2000; Bruckner et al. 2012), may be particularly sensitive to order 1-m water level changes. As revealed by a number of investigators, hydrodynamics over shallow reef crests are sensitive to water level changes (e.g., McDonald et al. 2006; Monismith et al. 2013; Lentz et al. 2016b, 2017). In a recent work, Lentz et al. (2017) found that the drag coefficient for depth-averaged flow over a platform reef strongly depends on mean water depth, varying by an order of magnitude over a depth range of 0.2–2 m. Furthermore, order 1-m water level variations will alter the thermal environment over shallow reef tops by changing the water volume influenced by surface heat flux over the reef crest (e.g., Davis et al. 2011).

Viewed as a function of frequency, the changes in Red Sea water level may be divided into three broad categories (illustrated in Fig. 2.4). Occupying the lowest-frequency cat-
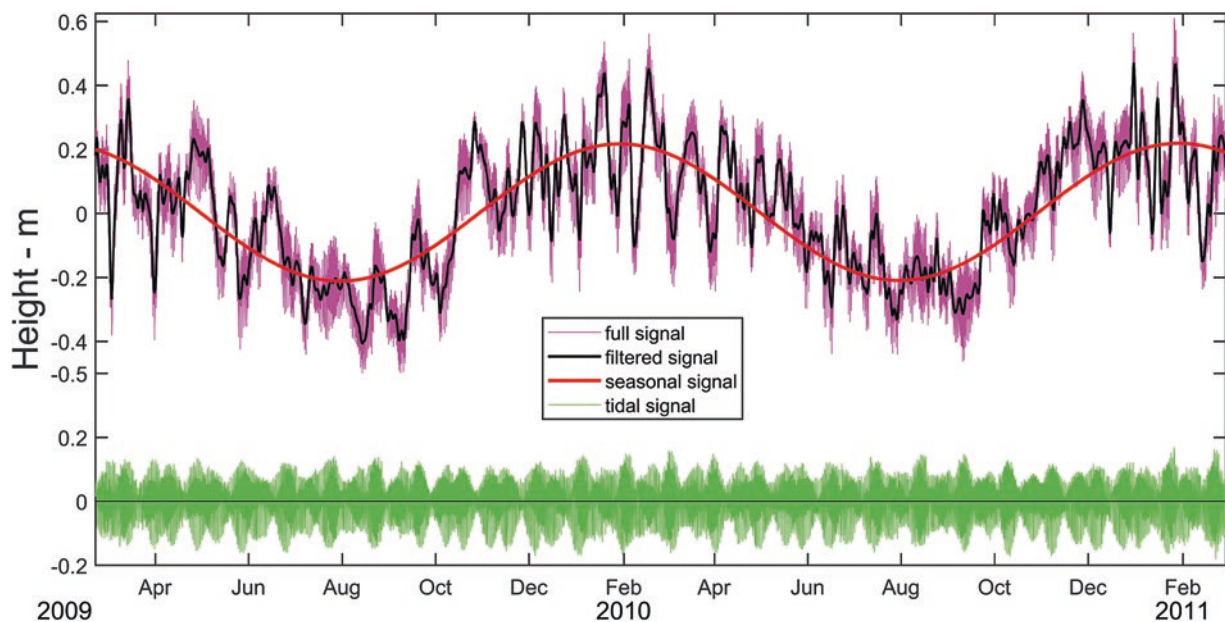

Fig. 2.4 The magenta line is a record of sea level height derived from pressure data acquired near Jeddah, SA (Fig. 2.1a). Other lines illustrate the three categories of sea level described in the text. The solid black line shows the pressure record filtered with a 66-hr half-power-point filter and encompasses the seasonal signal (red line) and the intermediate-frequency band signal (difference between the filtered and seasonal signal). The green line is the higher frequency signal (difference between the filtered and unfiltered signal), which is principally due to tidal motions

egory are motions varying over seasonal periods (>0.5 year), whereas the highest-frequency category is comprised principally of diurnal and semidiurnal tidal motions (periods <1.1 days). Sea level changes in the 'intermediate-frequency' category span a range of order 0.7 m and are contained in a period band of roughly 3–25 days. Current knowledge of sea level motions in each of these categories is reviewed below.

2.3.4.1 Seasonal Sea Level Variations

A number of researchers have reported on a seasonal signal of water level in the Red Sea marked by higher surface elevations in the winter than in the summer (Morcos 1970; Sultan et al. 1995b, 1996; Abdelrahman 1997; Sofianos and Johns 2001; Manasrah et al. 2009). Most observations of this phenomenon are from the central Red Sea (16.5–21.5°N) and show a seasonal sea level signal with a range of 0.3–0.4 m (illustrated in Fig. 2.4). Analysis of satellite-altimeter-derived sea surface height (SSH) data, indicate that the seasonal sea level range is roughly constant over the central and northern Red Sea, but declines in the southerly direction over the southern Red Sea to a magnitude of roughly 0.2 m near Bab al Mandab (Sofianos and Johns 2001). This trend is consistent with the analysis of Pazart (1974), who examined sea level records from a number of locations spanning the length of the Red Sea.

Numerous studies have considered the mechanisms driving the seasonal sea level variations in the Red Sea. Those factors most likely to contribute to the seasonal signal, based on dynamical considerations (i.e., momentum balance), are atmospheric pressure (i.e., the inverse barometer effect), surface wind stress and steric effects (variation in water density). As noted by Sultan et al. (1995a), atmospheric pressure is not likely to be of importance in driving the seasonal sea level signal because observed seasonal atmospheric pressure variations would produce a sea level response with a trend opposite to that observed (relatively high sea levels in summer). The analysis of Sofianos and Johns (2001), based on a simple 1-dimensional momentum balance (ignoring the Coriolis effect and bottom friction) with forcing by monthly wind stresses and variations in climatological water properties, indicates that the along-axis variation in wind stress is the principal driver of the seasonal sea level signal over all but the extreme southern portion of the Red Sea (south of 14°N) where the steric contribution dominates. The findings of Wahr et al. (2014), derived from combining SSH data, climatological sea water temperatures and GRACE (Gravity Recovery and Climate Experiment) mass data, are consistent with the dominance of wind forcing over steric effects in controlling the seasonal sea level variation over most of the Red Sea. However as opposed to Sofianos and Johns, Wahr et al. find that the steric influence on seasonal sea level is minimal over the southern Red Sea.

2.3.4.2 Intermediate Band Sea Level Variations

As compared with seasonal and tidal sea level motions (below), sea level variations in the intermediate frequency band (3–25 day periods) have received very little scientific attention. Reported analysis of intermediate band motions is largely confined to the examination of sea level records from Jeddah and Port Sudan (on opposite sides of the central Red Sea; Fig. 2.5) by Sultan et al. (1995a). Their analysis indicates statistically significant correlations between sea level variations at Jeddah and the along-shore wind stress, and between Port Sudan sea level variations and both the along- and across-shore wind stress components.

Despite the lack of scientific interest they have received thus far, sea level motions in the intermediate frequency band may be of importance for many environments, particularly over the crest of shallow platform reefs. As revealed by the analysis of pressure records taken near Jeddah, intermediate band sea level fluctuations include relatively large (order 0.6 m) water level changes occurring over periods of a few days (i.e., the changes seen in March 2009 in Fig. 2.4).

2.3.4.3 Tides

Considerable scientific attention was directed at Red Sea tides during the early twentieth century. Reviewed by Morcos (1970) and Defant (1961), much of this work entailed comparing theoretical calculations of tidal propagation throughout the Red Sea with tidal analysis of sea level data. A conclusion drawn by a number of investigators is that the tides over the Red Sea are predominantly co-oscillations with tides of the Gulf of Aden, with locally-forced, 'independent' tidal motions accounting for order 25% of the tidal amplitude. Cotidal charts, formulated based on the early twentieth century tidal analysis (Fig. 2.5), show an amphidromic point at roughly 20 °N, and tidal ranges increasing from less than 0.25 m over the central Red Sea to more than 0.5 m at the northern and southern extremes. As demonstrated by Vercelli (1925), Red Sea tides are predominately semidiurnal, with $[(K_1 + O_1)/(M_2 + S_2)] < 0.25$. An exception is within the nodal zone of the semidiurnal tide in the central Red Sea, where $[(K_1 + O_1)/(M_2 + S_2)]$ exceeds 0.5.

More recent tidal analyses of water level data from the central Red Sea are in agreement with tidal properties derived from the earlier work and clearly show the variation of tidal range with distance from the amphidromic point near 20 °N. The tidal signal measured at Port Sudan, close to the amphidromic point (Fig. 2.5), ranges over roughly 4 and 12 cm during the neap and spring tidal cycle, respectively (Eltaib 2010). This contrasts with the neap/spring tidal ranges measured at Jeddah (~15/35 cm; Sultan et al. 1995a) and Gizan (~20/120 cm; Eltaib 2010).

Fig. 2.5 Cotidal chart of the Red Sea (adapted from Morcos 1970). (**a**) The average tidal range in m. (**b**) Cotidal lines indicating the times of high water in hours after the transit of the moon at Greenwich
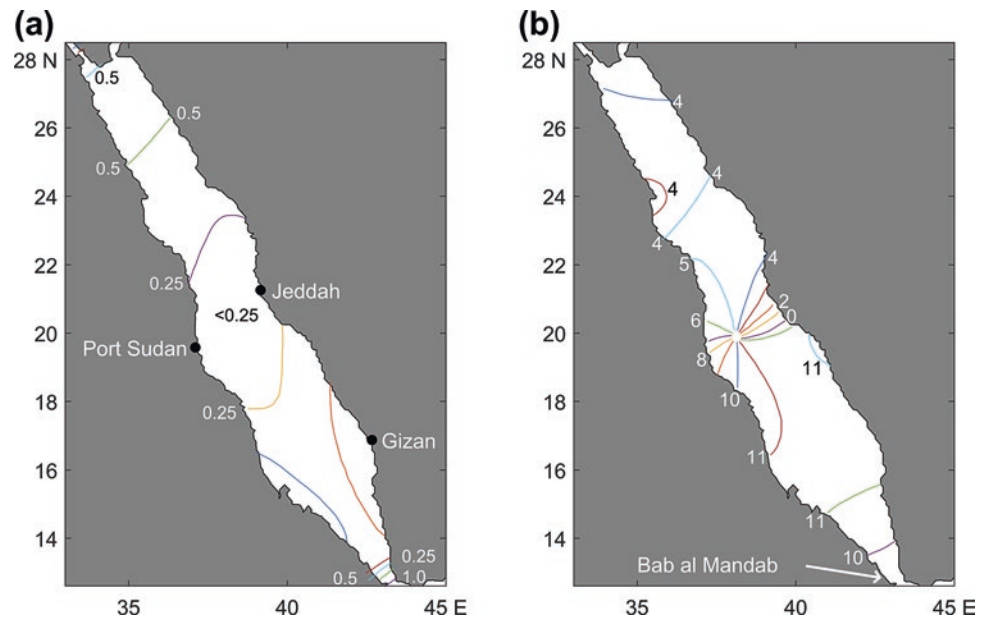
Tidal ranges at the southern extreme of the Red Sea, in the Strait of Bab al Mandab, are large and vary significantly over the length of the strait. Jarosz et al. (2005) report that the tidal range declines considerably going northward over the 150-km extent of the strait, from more than 1.5 m at Perim Narrows to less than 1 m at Hanish Sill. The character of the tidal signal also changes. Tidal energy at Perim Narrows is nearly evenly split between diurnal and semidiurnal bands, while more than 90% of the tidal energy at Hanish Sill is contained in the semidiurnal band. Earlier work by Vercelli (1925) indicates the presence of an M_2 tidal node in the central portion of the strait.

Reported analyses of tidal currents in the Red Sea are rare. Examination of ADCP velocity records by Churchill et al. (2014b) reveal particularly weak tidal velocities in the coastal zone of the central Red Sea (at ~22 $^\circ$N, see Fig. 2.1b). Consistent with the tidal analysis of water level data, these currents are predominately semidiurnal. Their magnitude seldom exceeds 8 cm s^{-1}.

The weak tidal flows in the central Red Sea reported by Churchill et al. contrast with strong tidal currents observed in the Strait of Bab al Mandab by Jarosz et al. (2005). These tidal flows reach magnitudes of ~1 m s^{-1} near the southern entrance of the strait, at Perim, and exceed 0.5 m s^{-1} further north at Hanish Sill. They are nearly rectilinear and oriented along the strait. Comparable in strength to the mean exchange flows, these tidal currents produce occasional reversals in the mean inflow and outflow through the strait. The analyses of Jarosz et al. (2005) further indicate that the tidal current in the strait includes a significant baroclinic component, which appears primarily in the diurnal band and is most energetic in winter.

Results of a numerical tidal model encompassing the Red Sea and the northern Gulf of Aden, reported by Madah et al.

(2015), reproduce many of the tidal features described above, including the dominance of the M_2 tide over most of the Red Sea, locations of tidal nodes, and the presence of strong tidal currents in the Strait of Bab al Mandab. The model results also show interesting, and potentially important, tidal features not yet confirmed by observations. These include strong tidal flows (peaking at order 0.3 m s^{-1}) oriented across isobaths in the coastal zone of the southern Red Sea (between 14 and 16°N; Figure 9 of Madah et al. 2015).

2.3.5 Surface Waves

The action of surface gravity waves has been shown to strongly impact the coastal environment. For example, numerous studies have indicated that the generation of bottom stress is often significantly enhanced by the interaction of near-bottom orbital currents due to surface waves with the more slowly varying flow (Cacchione and Drake 1982; Grant et al. 1984; Grant and Madsen 1986; Lyne et al. 1990; Madsen et al. 1993; Churchill et al. 1994; Chang et al. 2001). This enhancement can be appreciable at bottom depths as great as 100 m (Grant et al. 1984; Churchill et al. 1994). In addition, the breaking of surface waves at the edge of a shallow reef is a principal mechanism driving currents over the reef top (e.g., Symonds et al. 1995; Callaghan et al. 2006; Monismith 2007; Hench et al. 2008; Lowe et al. 2009; Vetter et al. 2010; Lentz et al. 2016b). This is due to a setup of sea-level elevation in the wave breaking zone, which in turn forces a across-reef current towards the protected (lee-side) of the reef (Monismith 2007; Hearn 2010; Lentz et al. 2016b).

Much of the current knowledge of the Red Sea wave climate has come from wave models that have been assessed by

comparison with the wave height series measured at the central Red Sea meteorological buoy (MB in Fig. 2.2) and wave properties derived from satellite-scatterometer data (Ralston et al. 2013; Langodan et al. 2014, 2016, 2017b; Aboobacker et al. 2017; Shanas et al. 2017a, b). These modeling studies have revealed some important large-scale features of the wind-driven wave field over the Red Sea. In the model results, much of the seasonal variability in the wave properties (height, direction and dominant period) in the Red Sea basin is linked to the seasonal variation in winds along the Red Sea axis (discussed in Atmospheric Setting). In the southern Red Sea, modeled waves are highest during November–April, when driven by the seasonal monsoon winds from the southeast. The monthly-averaged significant wave height (H_S = mean height of the highest third of the waves) during this period tends to be greatest in the 13–15.5 °N latitude band, reaching values close to 2 m (Ralston et al. 2013). In the northern and central Red Sea, modeled waves tend to propagate southeastward, generated by the persistent winds from the northwest. These waves are largest (with monthly mean H_S of 1.5–2 m) when 'strong northeasterly winds shifted the atmospheric convergence zone to the south' (Ralston et al. 2013). The dominant periods of the model-generated waves are predominantly in the 4–8 s range.

Numerous model results (Ralston et al. 2013; Langodan et al. 2016, 2017b; Aboobacker et al. 2017; Shanas et al. 2017b) indicate that the largest waves within the Red Sea are driven, not by the winds along the sea's axis, but by the cross-axial winds emerging from the Tokar Gap. As noted above (Atmospheric Setting), the Tokar Gap wind jet is a summer-time phenomenon associated with nocturnal discharge of cool air through the Tokar Gap. Ralston et al. (2013) find that waves generated by the Tokar Gap wind vary diurnally, with the largest waves (monthly-mean $H_S \sim 4$ m for July) occurring in the morning hours and the smallest waves (July mean $H_S < 0.5$ m) seen at night. The model results also indicate that the Red Sea wave field is impacted by winds flowing through mountain gaps along the northeastern Red Sea coast. The spatial scale over which these winds influence the modeled wave field is smaller than that of the Tokar Gap wind (~40 km vs. 100 km laterally, and ~100 km vs. 250 km along the jet).

While the modeling results reviewed above offer valuable information on the large-scale patterns of surface wave properties in the Red Sea, they have limited applicability to the Red Sea coastal areas, where wave propagation and attenuation are likely to be strongly influenced by small-scale and complex bathymetric features. A recent analysis of surface wave properties, derived using data from bottom-mounted ADCPs (Acoustic Doppler Current Profilers) and a meteorological buoy (Fig. 2.1), indicate that waves propagating from the deep basin into the coastal zone may be significantly attenuated as they move over the complex bottom topography characteristic of Red Sea coastal areas (Lentz et al. 2016a). The attenuation of wave height propagating shoreward over the coastal area examined by Lentz et al. is illustrated here by time series of H_S (Fig. 2.6) measured at an offshore meteorological buoy and three coastal sites: one (S2 in Fig. 2.1) on the outer portion of a 40–90-m deep 'plateau' situated between the Qita Dukais reef system and the
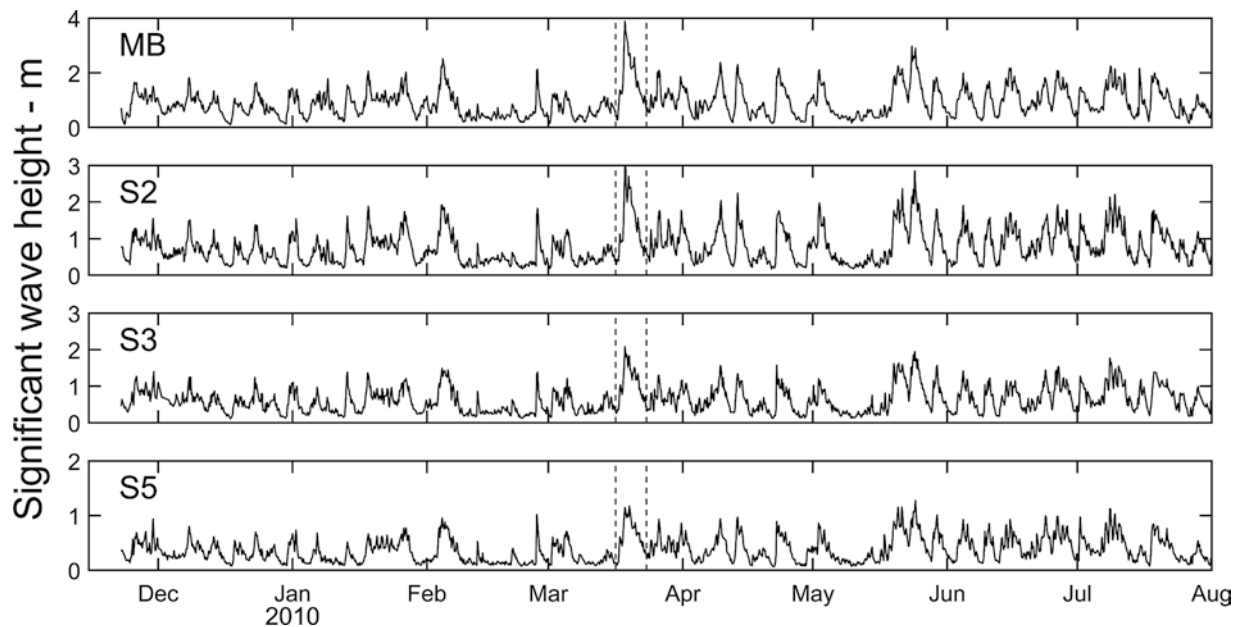

Fig. 2.6 Sample time series of significant wave height measured at locations shown in Fig. 2.1b. The vertical dashed lines bracket the event with the highest significant wave heights of the period shown

edge of the Red Sea basin and the other two (S3 and S5) within the reef system. These series are marked by frequent events in which peaks in H_S measured at the offshore buoy are matched by smaller peaks in the H_S series at the onshore sites that progressively decline in amplitude going shoreward into the plateau/reef system. This trend is nicely illustrated by the H_S measured during an event of particularly large waves in March 2010 (bracketed by dashed lines in Fig. 2.6). Over this event, maximum H_S declines from 3.9 m at the offshore buoy to values of 3.0, 2.1 and 1.2 m, respectively, at sites on the mid-plateau (S2), the outer edge of the Qita Dukais reef system (S3) and in the interior of the reef system (S5). A conclusion that may be drawn from the onshore decline in wave height, consistently seen in the H_s series, is that waves generated over the Red Sea basin are attenuated (to a greater extent than they are enhanced by wind-forcing) as they propagate onshore into the coastal/reef region. Nevertheless, reefs situated well onshore of the basin's edge can be exposed to significant wave energy. The H_S measured at site S5, which is roughly 12 km from the edge of the basin and at the edge of a platform reef, exceeds 0.5 m 26% of the time.

From analysis of pressure data on the platform reef adjacent to S5, Lentz et al. (2016a) show that wave transformation across the reef depends on incident wave height and reef depth. Incident waves with heights of >40% of reef depth break at the edge of the reef and decay gradually while propagating across the reef interior. Smaller incident waves, with heights <20% of the reef depth, propagate across the reef face without breaking but still gradually decay while moving across the reef interior. As demonstrated by Lentz et al. (2016b), wave breaking has a dominant impact in driving flows over the reef crest. From velocity and pressure data acquired over a platform reef in the central Red Sea, they find that breaking of waves on the seaward reef edge sets up a 2–10 cm elevation of sea level, which drives a 5–20 cm s⁻¹ current across the reef.

2.3.6 Water Properties

As noted above (Basin-scale Circulation), evaporation and surface heat exchange result in a north-south gradient of near-surface temperature and salinity along the Red Sea axis. In hydrographic survey data acquired during summer, near-surface temperature and salinity change from ~31.5 °C and 37.6 psu at the southern extreme of the Red Sea to ~27 °C and 40.5 psu at the northern extreme (Neumann and McGill 1962; Maillard and Soliman 1986; Sofianos and Johns, 2007). During winter, the near-surface temperature range is of order 24–28 °C, with the maximum temperatures tending to occur in the central Red Sea (near 19°N) (Quadfasel and Baudner 1993; Raitsos et al. 2013; Ali et al. 2018).

In most (or perhaps all) areas of the Red Sea, near-surface temperatures exhibit a seasonal variation (Raitsos et al. 2013; Churchill et al. 2014b; Ali et al. 2018). Recent work by Ali et al. (2018) reveals that the seasonal variations in near-surface temperature and salinity in the southern Red Sea (off of Port Sudan) are not the sole product of surface heat and mass fluxes, but also due to the alongshore advection of water with spatially varying temperature and salinity.

In the summertime hydrographic data, the seasonal thermocline typically begins in the upper 50 m and extends to order 150 m. The downward decline in temperature over seasonal thermocline is of order 8 °C, whereas the downward increase in salinity over the thermocline depth range is of order 0.5 psu. The observed wintertime temperature structure (Quadfasel and Baudner 1993) is characterized by a deep surface mixed layer, that can extend to order 150 m in the northern Red Sea, and a temperature decline of order 4 °C over the seasonal thermocline. In all seasons, the temperature and salinity show little variation beneath the seasonal thermocline, ranging over ~21.6–22 °C and 40.4–40.6 psu between ~200–2000 m depths (Neumann and McGill 1962; Maillard and Soliman 1986; Sofianos and Johns 2007).

Hydrographic data from the summer and autumn show the subsurface intrusion of GAIW. Driven northward through the Strait of Bab al Mandab by upwelling-favorable monsoon winds over the western Gulf of Aden (Patzert 1974), GAIW enters the southern Red Sea during summer (June–September) as a cold (17.4 °C at 75 m vs 31.4 °C in the top 10 m), fresh (35.8 vs 37.4 psu) and nutrient-rich (e.g., NO₃, 23.5 vs 0.9 μmol l⁻¹) intrusion typically contained in the 30–120-m depth range (Poisson et al. 1984; Maillard and Soliman 1986; Souvermezoglou et al. 1989). As documented by Sofianos and Johns (2007) and Churchill et al. (2014a), the temperature and salinity signal of GAIW extends a considerable distance northward of Bab al Mandab.

In addition to the large-scale patterns described above, the temperature/salinity fields of the Red Sea contain numerous small-scale features that may be of importance to reef growth and health. These include features associated with basin-scale eddies, coastal boundary currents (Bower and Farrar 2015; Eladawy et al. 2017), wind-driven upwelling (Churchill et al. 2014b; Fig. 2.3) and formation of a diurnal surface mixed layer. As demonstrated by Davis et al. (2011) and Pineda et al. (2013), diurnal variations in surface heat flux may produce a 'microclimate' over the shallow (<2-m depth) tops of platform reefs that are prevalent in the Red Sea coastal zone. Davis et al. show that daily temperature variations over the tops of 'protected' reefs (isolated from surface waves propagating from offshore) can be as high as 5 °C. Shallow reef environments may be particularly sensitive to long-term water temperature shifts associated with climate change. Through examination of satellite radiometer-

derived sea surface temperature data, Raitsos et al. (2011) document an abrupt increase in Red Sea surface temperatures, by ~0.7 °C, in the mid-1990's, with the warmer surface temperatures persisting to at least 2008. They attribute this shift to increases in air temperature associated with global climate trends.

2.3.7 Oxygen and Nutrients

The Red Sea basin may be characterized as oligotrophic (Stambler 2005) owing in part to the limited supply of nutrients delivered to the Red Sea through terrestrial runoff. It is well established that principal source new water-borne nutrients to the Red Sea is the summertime intrusion of GAIW (Khimitsa and Bibik 1979; Souvermezoglou et al. 1989). As demonstrated by Souvermezoglou et al. (1989), the seasonality of the GAIW intrusion results in a seasonal variation of the Red Sea nutrient budget, marked by a net nutrient gain in the summer and loss in the winter.

Analysis of data from a September 2011 hydrography cruise of the central and northern Red Sea by Churchill et al. (2014a) indicates that GAIW is distributed broadly through the Red Sea. Churchill et al. identify four modes of GAIW transport: (1) transit of nutrient-rich (NO_3 up to 19 μmol l^{-1}) GAIW through the southern Red Sea (to 19°N) in a subsurface current flowing along the eastern basin margin with a speed of ~25 cm s^{-1}, (2) movement of GAIW across the Red Sea basin in the circulation of basin-scale eddies, (3) northward flow of GAIW over the central and northern Red Sea (identifiable to 24 °N), and (4) incursion of GAIW into coastal reef systems. In view of the fourth mode, Churchill et al. note that GAIW could be an important source of new nutrients to coral reef ecosystems, particularly in the southern Red Sea where nutrient concentrations in GAIW have been observed at the highest concentration (Poisson et al. 1984; Sofianos and Johns 2007). Churchill et al. also observe that the high nutrient concentrations within GAIW extend into the euphotic zone and appear to fuel enhanced productivity over depths of 35–67 m. In the absence of GAIW, near-surface Red Sea water typically contains low nutrient concentrations (i.e., $NO_3 < 1$ μmol l^{-1}) in the upper 70–120 m (Morcos 1970; Poisson et al. 1984; Sofianos and Johns 2007; Churchill et al. 2014a; Triantafyllou et al. 2014).

Analysis of more recent data, from a November 2013 cruise, by Zarokanellos et al. (2017a) also reveal the presence of GAIW in the central Red Sea. Consistent with the notion that GAIW fuels productivity, the GAIW water parcels observed by Zarokanellos et al. contain elevated concentrations of chl-a and colored dissolved organic matter relative to surrounding water.

Beneath the surface 120 m, vertical nutrient profiles from the Red Sea are marked by a concentration maximum ($NO_3 > 15.5$ μmol l^{-1}) in the 300–650-m depth range (Neumann and McGill 1962; Morcos 1970; Poisson et al. 1984; Weikert 1987). The magnitude of the maximum concentration tends to increase going from northern Red Sea (maximum $NO_3 = 15.5$–18.0 μmol l^{-1}) to the southern Red Sea (maximum $NO_3 = 18.9$–22.1 μmol l^{-1}) (Weikert 1987). This trend is likely due to the accumulation of dissolved nutrients by remineralization of sinking particles in the layer encompassing the nutrient maximum as it flows southward from its formation region in the northern Red Sea to Bab al Mandab.

Because there is a tight inverse relationship between concentrations of dissolved nutrients and dissolved oxygen (DO), as indicated by a positive correlation between nutrient concentration and apparent oxygen utilization (Naqvi et al. 1986; Churchill et al. 2014a), the distribution of nutrients described above is closely associated with the distribution of DO in the Red Sea. For example, DO distributions along the Red Sea axis show a vertical minimum in the 300–650-m depth range of the nutrient maximum as well as a north-to-south increase in DO in this depth range (Neumann and McGill 1962; Poisson et al. 1984; Sofianos and Johns 2007).

A noteworthy feature of the nutrient mix within the Red Sea is the large departure of nutrient-to-nutrient ratios from open ocean (Redfield) values. Analysis of nutrient data by Naqvi et al. (1986) gives carbon:nitrogen:phosphorus (C:N:P) ratios of 188:21:1, considerably different from the Redfield ratios of 106:16:1. Grasshoff (1969) reports a similar excess of N over P (relative to open ocean proportions). Navqi et al. note that this N:P 'imbalance' cannot be attributed to the properties of the influx through Bab al Mandab, as the Gulf of Aden source water of this influx has N:P ratios close to the Redfield value. Using available estimates of flows and nutrient concentrations though Bab al Mandab, Navqi et al. computed a net 0.74×10^{12} g year^{-1} outflow of N from the Red Sea, similar to a later estimate by Bethoux (1988). Navqi et al. posit that the excess N exported from the Red Sea could be the result of fixation of nitrogen (entering the Red Sea from the atmosphere) by the cyanobacteria *Trichodesmium*, which is prevalent in the Red Sea. However, later calculations by Bethoux (1988) indicate that nitrogen fixation by open-water blooms of *Trichodesmium* likely accounts for only a small fraction of the imbalance of the Red Sea N budget. Bethoux finds that fixation by coral reef communities is a more probable mechanism for generating the excess N. Nitrogen fixation by Red Sea coral communities has been observed by El-Shenawy and El-Samra (1996) and Grover et al. (2014). The observations of El-Shenawy and El-Samra indicate that nitrogen fixation over reefs in the northern Red Sea and Gulf of Suez tends to occur at a greater rate during the daylight (vs. nighttime) hours and during summer (vs. spring and winter).

2.3.8 Light and Chlorophyll Distribution

The productivity and distribution of reef-building corals is highly dependent on the ambient light environment. The quantity of light to which corals are exposed is a function of the surface irradiance and the degree to which this is attenuated through the water column. Measurements of Red Sea light levels come predominately from the northern Red Sea and the Gulf of Aqaba. Winters et al. (2009) show that levels of surface irradiance in this region are exceptional high, exceeding surface irradiance levels over reef environments off of Mexico, Australia and Hawaii by order 40%. The seasonal variation of surface irradiance over the Gulf of Aqaba is significant, with maximum daily global irradiance ranging from ~550 W m^{-2} over November-January to ~950 W m^{-2} over April–July (Stambler 2006; Winters et al. 2009).

The exceptionally clear water of the Red Sea allows for deep penetration of incident light. Measurements analyzed by Stambler (2005, 2006) show that the euphotic zone depth (beyond which the downwelling shortwave radiation is <1% of the surface irradiance) in the northern Red Sea and Gulf of Aqaba ranges over 74–115 m. Raitsos et al. (2013) report a slightly narrower euphotic zone depth range of 77–96 m based on measurements from the central Red Sea (near 22 °N). The degree of light penetration in the northern Red Sea appears to vary with season. Stambler (2006) reports that the exponential attenuation coefficient for PAR [$K_d(PAR)$] measured in the Gulf of Aqaba ranges from a summertime minimum of 0.04 m^{-1} to a springtime maximum of 0.064 m^{-1}. The penetration of light into Red Sea also varies significantly as a function of wavelength, with minimum attenuation experience by blue light (Stambler 2006; Mass et al. 2010; Roder et al. 2013). Based on light measurements in the Gulf of Aqaba, Mass et al. (2010) report attenuation coefficients of 0.056 m^{-1} and 0.449 m^{-1} for blue (490-nm wavelength) and red (665 nm), respectively. In their data set, no light with wavelength > 600 nm appears at 40 m depth. They present evidence that coral colonies of *Stylophora pistillata* are capable of photoadaptation to the differing light conditions with depth. Specifically, they show the photosynthetic performance for colonies acquired from depths of 3 and 40 m is maximal when illuminated with full-PAR and filtered blue light, respectively.

As documented by Fricke and Knauer (1986) and Fricke et al. (1987), zooxanthellate corals may occur in the dimly-lit twilight zone beneath the euphotic zone. The observations of Fricke and Knauer (1986) reveal corals in the 100–200 m depth range where they are exposed to 0.1–1.7% of surface irradiance.

The vertical distribution of chl-*a* is principally controlled by combination of PAR and available nutrients, and is typically marked by a 'deep maximum' at the base of the main pycnocline. Fluorometer measurements taken from the cen-

tral and northern Red Sea show the deep chl-*a* maximum occurring over a depth range of ~40–140 m (Churchill et al. 2014b; Zarokanellos et al. 2017a, b). During the autumn, the spatial variation of the maximum chl-*a* concentration seen in this depth range appears to be related to the distribution of the seasonal GAIW intrusion, with maximum chl-*a* concentrations tending to decrease going from south to north (presumably due to the dilution and uptake of nutrients borne by the GAIW intrusion as it is advected northward) and from east to west (reflecting the tendency of the GAIW intrusion to flow along the eastern margin of the Red Sea basin) (Churchill et al. 2014b; Zarokanellos et al. 2017a).

As revealed by analysis of satellite spectroradiometer measurements (Acker et al. 2008; Raitsos et al. 2013; Abdulsalam and Majambo 2014), the near-surface chl-*a* field in the Red Sea (above the deep chl-*a* maximum) exhibits a distinct seasonal and spatial signal. Over the entire Red Sea, near-surface chl-*a* concentrations tend to be highest in winter (Oct.-Mar.) and lowest in summer (May-Aug.). Raitsos et al. (2013) attribute the low near-surface chl-*a* concentrations of summer to the strong summertime stratification blocking the upward transfer of deep nutrients. They postulate that the high near-surface chl-a concentrations of winter are the result of vertical mixing of nutrients in the north and the productivity associated with GAIW-borne nutrients in the south. In all seasons, the near-surface chl-*a* concentrations tend to be highest in the southern Red Sea (south of 17.5°N), exceeding concentrations of the northern Red Sea (north of 22°N) by an order of magnitude. However, as shown by Acker et al. (2008), the surface chl-*a* field observed in the northern Red Sea during the winter/spring bloom period can be strongly heterogeneous with relatively high chl-*a* concentrations (up to 5 mg m^{-3}) appearing in small-scale filaments.

2.4 The Carbonate System

With the notable exception of riverine input, the mechanisms that govern the inorganic carbonate chemistry in the Red Sea are similar to those that control typical coastal and continental shelf environments. These mechanisms include air-sea gas exchange, primary productivity and respiration, and formation and dissolution of CaCO$_3$ minerals. However, the distinct climatological, geological and hydrographic settings of the Red Sea produce some unique carbonate system characteristics specific to this basin.

The shallow (approximately 140-m deep) sill of the Strait of Bab al Mandab (Fig. 2.1) limits the passage of deep Indian Ocean water into the Red Sea. As a result, the water entering the basin is predominately surface seawater, which contains relatively low levels of dissolved inorganic carbon (DIC) and nutrients. The exception is the summer-time intrusion of GAIW, which is the primary source of water-borne nutrients

to the Red Sea. The limited supply of nutrients renders the Red Sea oligotrophic with primary production rates of 20–60 mmol C m^{-2} d^{-1} (Klinker et al. 1976; Lazar et al. 2008; Qurban et al. 2014). The high evaporation rates in the Red Sea (~ 2 m year^{-1}) concentrate dissolved ions in the surface water (Steiner et al. 2014). As a result, the measured DIC range in the Red Sea of 2000–2200 µmol kg^{-1} (Weiss et al. 1983; Papaud and Poisson 1986; Krumgalz et al. 1990; Wurgaft et al. 2016) is considerably higher than the salinity normalized DIC (nDIC = DIC*35/salinity) range, which spans 1790 to 1960 µmol kg^{-1}. Consequently, the measured DIC falls within the range of DIC in the world oceans (~2000–2300 µmol kg^{-1}; Emerson and Hedges 2008), whereas the salinity normalized DIC is considerably lower.

The vertical distribution of DIC in the Red Sea resembles that of pelagic environments. It is characterized by low DIC levels in the upper parts of the water column (Fig. 2.7), resulting from photosynthetic CO$_2$ uptake and air-sea gas exchange, and higher DIC concentration below the photic zone, due to bacterial re-mineralization of organic material. A DIC maximum is typically seen at ~ 300 m. An exception is the northern Gulf of Aqaba (GOA, Fig. 2.1) DIC distribution during winter (Fig. 2.8). The water column in this part of the Red Sea is subject to deep vertical mixing, occasionally mixing to the bottom (Genin et al. 1995; Lazar et al. 2008). However, even in the stratified center of the Red Sea, the difference between the shallow and deep-water nDIC is smaller than 100 µmol kg^{-1} (Fig. 2.8), whereas in the adjacent Gulf of Aden this difference exceeds 200 µmol kg^{-1} (Talley 2013). The relatively low DIC concentrations in the deep Red Sea

are principally the result of two factors. The first is the short residence time (~ 40 year) of Red Sea deep water (Cember 1988), which limits the accumulation time of respiration products below the thermocline. The second is the low primary productivity rates of the oligotrophic Red Sea. This results in low rates of downward export of organic material from the photic zone, which reduces the accumulation potential of DIC in Red Sea deep water.

The distribution of total alkalinity (TA) in the Red Sea is affected by evaporation, CaCO$_3$ precipitation and organic matter remineralization. The TA of the Red Sea surface water varies between 2300–2600 µmol kg^{-1} (Weiss et al. 1983; Steiner et al. 2014), and increases from south to north due to evaporation (Weiss et al. 1983). However, as shown by Steiner et al. (2014), this increase is not conservative due to biological CaCO$_3$ sequestration that removes alkalinity from the seawater. As a result, the salinity normalized alkalinity (nTA = TA*35/salinity) in the Red Sea is approximately 2100 µmol kg^{-1}, considerably lower than typical TA in the surface ocean (~2300 µmol kg^{-1}, Millero et al. 1998). Moreover, nTA shows a south to north decrease, opposite to the trend of TA. Based on the deviation of TA from conservative behavior and the accompanying increase in the Sr/Ca ratios, Steiner et al. (2014) estimate that the rate of CaCO$_3$ production in the Red Sea is 7 × 10^{10} kg year^{-1}, and that 80% of this production is attributed to pelagic calcareous plankton with the remaining 20% attributed to coral-reef growth.

The vertical distribution of TA in the Red Sea exhibits a unique pattern. In contrast to the typical continental shelf and pelagic environments, where TA increases with depth
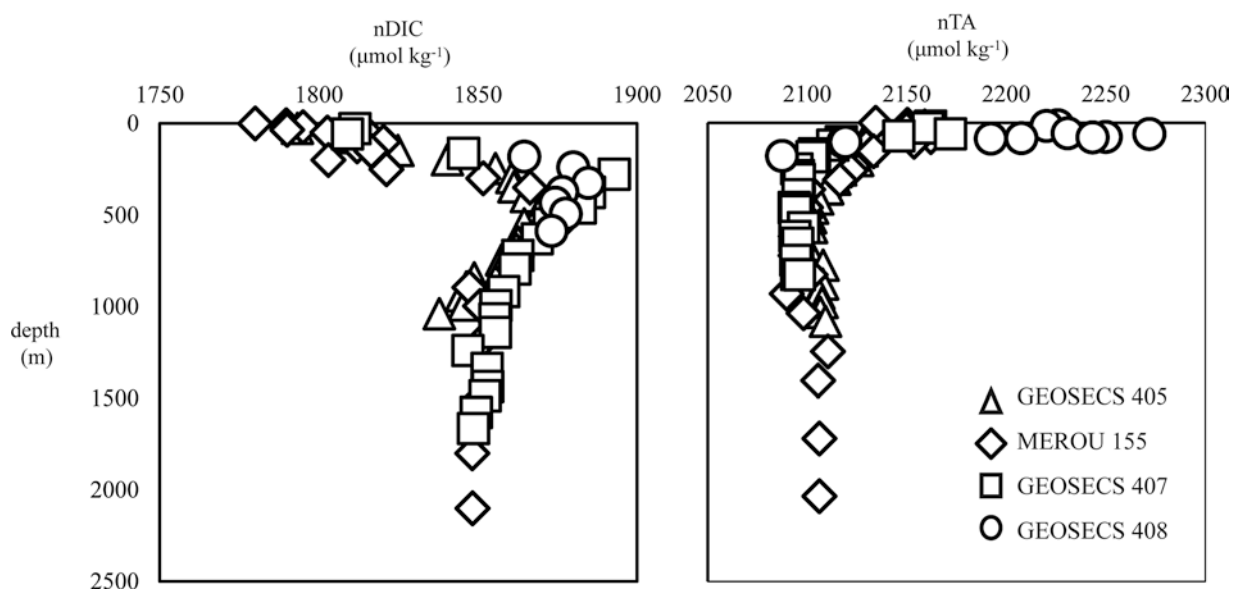

Fig. 2.7 Dissolved inorganic carbon (nDIC) and alkalinity (nTA) data from the Red Sea basin (see Fig. 2.1a for the locations). All data shown are normalized to a salinity of 35 (see text). nDIC shows a typical oceanic profile, with higher nDIC concentrations below the photic zone. The difference in nDIC between the surface and the deep water, however, is considerably smaller than the corresponding difference in the ocean (see text). The vertical distribution of nTA, however, is opposite the the typical oceanic distribution, with lower values in the deep water
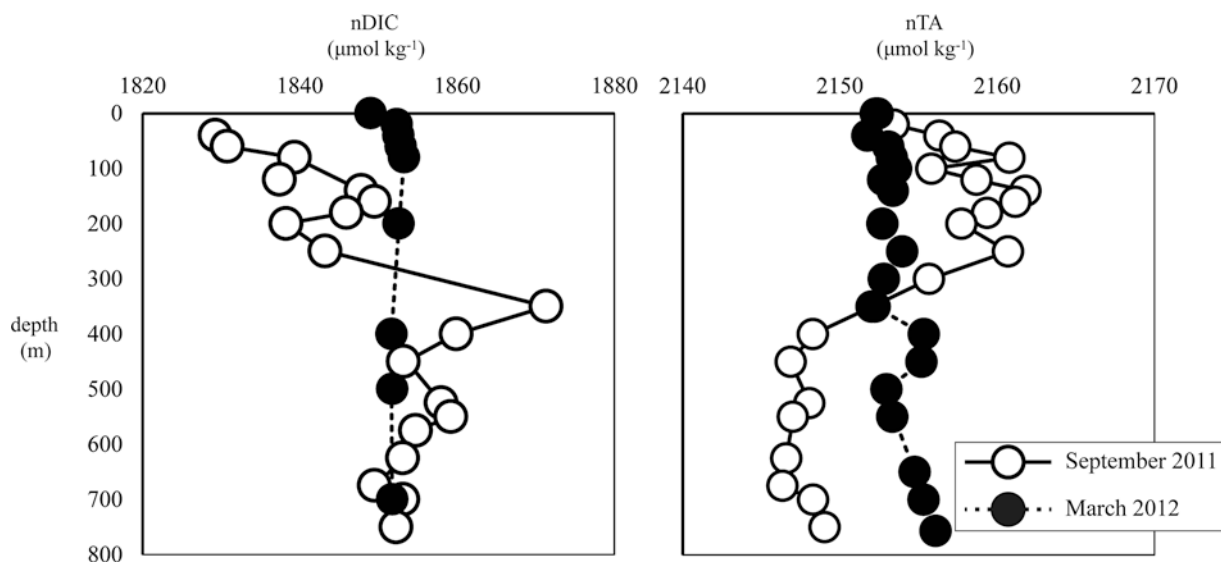
Fig. 2.8 Dissolved inorganic carbon (nDIC) and alkalinity (nTA) data from the northern Gulf of Aqaba (GOA, Fig. 2.1a). All data shown are normalized to a salinity of 35 (see text). The September 2011 profiles are representative of thermally stratified water column (usually between April and October), whereas the March 2012 profiles represent mixed water column. Note that the water column does not mix to the bottom of the northern GOA every winter. However, the mixed layer depth usually exceeds 200 m

due to $CaCO_3$ dissolution (Broecker and Takahashi 1978; Broecker et al. 1982), nTA in the Red Sea decreases with depth (Fig. 2.8). A substantial difference between the deep Red Sea and the deep ocean is that unlike the deep ocean, where the water temperatures are ~ 4 °C, the temperature of the deep Red Sea water is ~20 °C. This high temperature has an important effect on the stability of $CaCO_3$ minerals (calcite and aragonite). Because the solubility of $CaCO_3$ minerals decreases at high temperatures (Mucci 1983), the warm temperature of the Red Sea deep water, combined with its relatively high TA:DIC ratios, maintains a high degree of $CaCO_3$ saturation. The degree of saturation is commonly expressed as $\Omega = [Ca^{2+}][CO_3^{2-}]/K_{SP}$, where $[Ca^{2+}]$ and $[CO_3^{2-}]$ are the measured concentrations of Ca^{2+} and CO_3^{2-}, and K_{SP} is the solubility product for either calcite or aragonite. In the Red Sea, Ω is >1 over the entire water column, indicating supersaturated conditions with respect to $CaCO_3$ minerals, whereas in most parts of the ocean Ω values are <1 below a certain depth (the 'lysocline'). Ω values in the Red Sea range over 4.6–6.7 and 3.1–4.4, for calcite and aragonite, respectively. The lowest deep-water Ω values in the Red Sea are 3.2 and 2.2, for calcite and aragonite, respectively (calculations for this chapter were conducted using the CO_2-SYS program, Pierrot et al. 2006). As a result, $CaCO_3$ minerals do not dissolve in the water column of the Red Sea. While this explains the lack of TA increase with depth, it does not account for the observed decrease with depth. The alkalinity "deficiency" in the deep water can be partially explained by the fact that the Red Sea deep water forms in the northern Red Sea (Plahn et al. 2002) where the nTA is lower due to $CaCO_3$ sequestration (Steiner et al. 2014). However, this deficiency is appar-

ent even in the northern Gulf of Aqaba (Fig. 2.8). The accumulation of NO_3^- and PO_4^{3-} by respiration can decrease nTA (Brewer and Goldman 1976). However, Wurgaft et al. (2016) show that the deep water TA deficiency is significant even if the nTA is corrected to account for the increase in NO_3^- and PO_4^{3-}. Moreover, Wurgaft et al. note that nTA in the deep Red Sea decreases from north to south, and that this horizontal distribution is significant when nTA is corrected for the addition of nutrients. Wurgaft et al. hypothesize that the north-south decrease in deep-water nTA stems from heterogeneous $CaCO_3$ precipitation on sinking particles, mainly dust and biogenic $CaCO_3$ from the photic zone. However, this hypothesis has yet to be thoroughly examined.

Notably, the behavior of the carbonate system parameters over the Red Sea coral-reefs can be very different from that of the adjacent open-water. For example, the carbonate system parameters over coral-reefs are subject to large diurnal cycle, whereas the diurnal variations in the open-sea are negligible. Silverman et al. (2007) show that biological $CaCO_3$ production induces a 20 μmol kg^{-1} difference between the TA in the open-water and the TA in the back lagoon of the coral reef in the northern Gulf of Aqaba. The amplitude of the diurnal TA cycle is similar, mainly because the main mechanism that increases the TA over the coral-reef is water exchange with the open-sea. Notwithstanding, Silverman et al. (2007) find that unlike the open-sea, where $CaCO_3$ minerals are stable, $CaCO_3$ dissolution constitutes an important mechanism in the diurnal nTA cycle over the coral reef.

An important issue that has not been addressed in the scientific literature is the effect that long-term changes in the Red Sea carbonate system may have on coastal reef

ecosystems. In particular, the process of 'ocean acidification' (Orr et al. 2005), the global decrease in the sea water pH and CO_3^{2-} levels (Dore et al. 2009; Bates 2007), may have severe implications on the flourishing coral-reefs of the Red Sea. Reduction in pH and CO_3^{2-} levels has been shown to retard $CaCO_3$ precipitation in many calcifying organisms, such as planktonic foraminifera (De Moel et al. 2009; Moy et al. 2009), coralline algae (Kuffner et al 2008) and corals (Cooper et al. 2008; Silverman et al. 2012). It is believed that the slowing of precipitation in corals is due to the sensitivity of the enzymes involved in the $CaCO_3$ precipitation pathway to a decrease in pH or CO_3^{2-} (Erez et al. 2011). The future impact of ocean acidification on the global coralline ecosystem is estimated to be harsh (e.g., Gattuso et al. 1998; Silverman et al. 2009), with a potential threat of a global collapse of this ecosystem (Erez et al. 2011). Given the lack of recent published data on the carbonate system of the Red Sea, the full extent of acidification within the Red Sea and its impact on Red Sea corals are unknown. A process that may locally mitigate acidification is the dissolution of $CaCO_3$ minerals in sediments. Whereas this process is deemed to be an insignificant buffer mechanism on a global scale (Andersson et al. 2003), it may be important in certain areas of the Red Sea due to the abundance of soluble, Mg-rich carbonates in the Red Sea sediments (Luz et al. 1984) and intense vertical mixing (that would increase the interaction between seawater and sediments), as occurs during winter in the northern Red Sea. However, given the dearth of recent carbonate measurements from the Red Sea, the extent to which this process may locally stem acidification is uncertain.

Carbonate chemistry may also be impacted at a local scale by the seasonal intrusion of GAIW. As noted above, GAIW has been observed flowing into the coastal reef system of the southern Red Sea. However, because there a few published measurements of the carbonate properties of GAIW (Morcos 1970; Grasshoff 1969), the impact of GAIW Red Sea carbonate chemistry is unknown.

2.5 Summary and Conclusions

It is evident from the above literature review that ongoing research is giving an increasingly complex view of the Rea Sea system. As a case in point, the impacts of mountain gap winds on the Red Sea were not considered in the scientific literature until roughly 10 years ago. Since that time, modeling studies have demonstrated that winds emerging from mountain gaps onto the Red Sea can have magnitudes exceeding 20 m s^{-1}, cover a significant fraction of the Red Sea surface area, and generate surface waves with significant wave heights of order 4 m. Furthermore, it has been shown that the passage of mountain gap winds over the northern Red Sea during winter results in intensive heat loss to the atmosphere. As such, these winds may be of particular importance in the surface buoyancy loss that leads to the formation of Red Sea Overflow Water. Mountain gap winds have also been identified as a principal (but not the sole) mechanism for generating mesoscale eddies.

Recent studies reviewed above have revealed the dominance of mesoscale eddies and coastal currents in the surface height and near-surface circulation fields. As shown by the analysis of recent cruise data, these circulation features appear to be important in transporting GAIW, the principal source of water-borne nutrients to the Red Sea, over much of the length and breadth of the Red Sea. Furthermore, recent modeling studies have indicated that mesoscale eddies may appreciably influence Red Sea Overflow Water formation and the overturning flow structure of the Red Sea.

As reviewed above, understanding of the light field of the Red Sea environment has been furthered by recent investigations. Modeling has shown that the dust storms that frequent the Red Sea region can significantly attenuate the incoming shortwave radiation, by up to 100 w m^{-2}. Observations in the northern and central Red Sea have quantified the deep penetration of incident light (with euphotic zone depths exceeding 100 m) and shown that coral colonies are capable of adapting to the changes in the distribution of light wavelength with increasing depth.

Other recent advances in the understanding of the Red Sea system reviewed above include (but are not limited to): demonstrating that the seasonal signal of Red Sea surface level is linked to the seasonal variation of the along-axis wind stress, documenting the seasonal and spatial variations of the near-surface chlorophyll distribution, quantifying and modeling the flows and temperature variations over platform reef tops, and estimating the rate of $CaCO_3$ production in the Red Sea and its partition between production of pelagic calcareous plankton and coral-reef growth.

However, despite recent advances, it is clear from the above review that understanding of many critical processes in the Red Sea system is limited. While a full list of such processes would overburden this chapter, a few examples are worth noting. Little is known as to how mesoscale eddies may affect shelf-basin water exchange or promote primary productivity through upward deflection of density/nutrient surfaces. There is still considerable uncertainty regarding the processes that produce the 'excess' nitrogen (relative to phosphorus) observed in the Red Sea. The role of dust deposition in altering the chemical properties (i.e., nutrient concentration and $CaCO_3$ saturation) of the Red Sea has yet to be investigated. Perhaps the most critical process for which further research is warranted is the manner in which the Red Sea carbonate system is responding, and will respond, to long-term changes in atmospheric conditions, most notably air temperature and CO_2 concentration.

References

Abdelrahman SM (1997) Seasonal fluctuations of mean sea level at Gizan, Red Sea, 2009. J Coast Res 13:1166–1172

Abdulsalam A, Majambo G (2014) Remote sensing of phytoplankton distribution in the Red Sea and Gulf of Aden. Acta Oceanol Sin 33(9):93–99. https://doi.org/10.1007/s13131-014-0527-1

Aboobacker VM, Shanas PR, Alsaafani MA, Albarakati AMA (2017) Wave energy resource assessment for Red Sea. Renew Energy 114A:46–58

Acker J, Leptoukh G, Shen S, Zhu T, Kempler S (2008) Remotely-sensed chlorophyll a observations of the northern Red Sea indicate seasonal variability and influence of coastal reefs. J Mar Syst 69:191–204

Ahmad F, Sultan SAR, Moammar MO (1989) Monthly variations of net heat flux at the air-sea interface in coastal waters near Jeddah, Red Sea. Atmos Ocean 27(2):406–413. https://doi.org/10.1080/07055900.1989.9649343

Ali EB, Churchill JH, Barthel K, Skjelvan I, Omar AM, de Lange TE, Eltaib E (2018) Seasonal variations of hydrographic parameters off the Sudanese coast of the Red Sea, 2009–2015. Reg Stud Mar Sci 18:1–10. https://doi.org/10.1016/j.rsma.2017.12.004

Almogi-Labin A, Hemleben C, Meischner D, Erlekeuser H (1991) Paleoenvironmental events during the last 13000 years in the Central Red Sea as recorded by pteropoda. Paleoceanography 6:83–98

Almogi-Labin A, Edelman-Furstenberg Y, Hemleben C (2008) Variations in the biodiversity of thecosomatous pteropods during the Late Quarternary as a response to environmental change in the Gulf of Aden – Red Sea – Gulf of Aqaba ecosystem. In: Por FD (ed) Aqaba-Eilat, the improbable Gulf. The Hebrew University Magnes Press, Jerusalem, pp 31–49

Al-Rifaiy IA, Cherif OH (1988) The fossil coral reefs of Al-Aqaba, Jordan. Facies 18:219–230

Andersson AJ, Mackenzie FT, Ver LM (2003) Solution of shallow-water carbonates: an insignificant buffer against rising atmospheric CO_2. Geology 31:513–516

Arz HW, Lamy F, Ganopolski A, Nowaczyk N, Pätzold J (2007) Dominant Northern Hemisphere climate control over millennial-scale glacial sea-level variability. Quat Sci Rev 26:312–321

Bates NR (2007) Interannual variability of the oceanic CO_2 sink in the subtropical gyre of the North Atlantic Ocean over the last 2 decades. J Geophys Res Oceans 112:C9013–C9039

Ben-Avraham Z, Almagor G, Garfunkel Z (1979) Sediments and structure of the gulf of Elat (Aqaba) - Northern Red Sea. Sediment Geol 23:239–267

Bethoux JP (1988) Red Sea geochemical budgets and exchanges with the Indian Ocean. Mar Chem 24:83–92

Biton E, Gildor H, Peltier WR (2008) Red Sea during the last glacial maximum: implications for sea level reconstruction. Paleoceanography 23:PA1214

Biton E, Trommer G, Siccha M, Kucera M, van der Meer MTJ, Schouten S (2010) Sensitivity of Red Sea circulation to monsoonal variability during the Holocene: an integrated data and modeling study. Paleoceanography 25:PA4209

Bohannon RG (1986) Tectonic configuration of the Western Arabian continental margin, southern Red Sea. Tectonics 5:477–499

Bonatti E (1985) Punctiform initiation of seafloor spreading in the Red Sea during transition from a continental to an oceanic rift. Nature 316:33–37

Bosworth W, Huchon P, McClay K (2005) The Red Sea and Gulf of Aden basins. J Afr Earth Sci 43:334–378

Bower AS, Farrar JT (2015) Air–Sea interaction and horizontal circulation in the Red Sea. In: Rasul NMA, Stewart ICF (eds) The Red Sea, Springer earth system sciences. Springer, Berlin/Heidelberg, pp 349–342. https://doi.org/10.1007/978-3-662-45201-1_19

Braithwaite CJR (1987) Geology and paleogeography of the Red Sea region. In: Edwards AJ, Head SM (eds) Red Sea. Pergamon Press, pp 22–44

Brewer PG, Goldman JC (1976) Alkalinity changes generated by phytoplankton growth. Limnol Oceanogr 21:108–117

Brindley H, Osipov S, Bantges R, Smirnov A, Banks J, Levy R, Jish Prakash P, Stenchikov G (2015) An assessment of the quality of aerosol retrievals over the Red Sea and evaluation of the climatological cloud-free dust direct radiative effect in the region. J Geophys Res Atmos 120:10,862–10,878. https://doi.org/10.1002/2015JD023282

Broecker WS, Takahashi T (1978) Relationship between Lysocline depth and Insitu carbonate ion concentration. Deep-Sea Res 25:65–95

Broecker WS, Peng T-H, Beng Z (1982) Tracers in the Sea. Lamont-Doherty Geological Observatory, Columbia University, Palisades, pp 58–93

Bruckner A, Rowlands G, Riegl B, Purkis S, Williams A, Renaud P (2012) Khaled bin Sultan Living Oceans Foundation Atlas of Saudi Arabian Red Sea marine habitats. Panoramic Press, Phoenix, p 262

Cacchione DA, Drake DE (1982) Measurements of storm-generated bottom stresses on the continental shelf. J Geophys Res 87:1952–1960

Callaghan DP, Nielsen P, Cartwright N, Gourlay MR, Baldock TE (2006) Atoll lagoon flushing forced by waves. Coast Eng 53:691–704. https://doi.org/10.1016/j.coastaleng.2006.02.006

Cember RP (1988) On the sources, formation, and circulation of Red-Sea deep-water. J Geophys Res Oceans 93:8175–8191

Chang GC, Dickey TD, Williams AJ III (2001) Sediment resuspension over a continental shelf during Hurricanes Edouard and Hortense. J Geophys Res 106:9517–9531

Chen C et al (2014) Process modeling studies of physical mechanisms of the formation of an anticyclonic eddy in the Central Red Sea. J Geophys Res Oceans 119:1445–1464. https://doi.org/10.1002/2013JC009351

Churchill JH, Wirick CW, Flagg CN, Pietrafesa LJ (1994) Sediment resuspension over the continental shelf east of the Delmarva Peninsula. Deep-Sea Res Part II 41(2/3):341–363

Churchill JH, Bower AS, McCorkle DC, Abualnaja Y (2014a) The transport of nutrient-rich Indian Ocean water through the Red Sea and into coastal reef systems. J Mar Res 72:165–181. https://doi.org/10.1357/002224014814901994

Churchill JH, Lentz SJ, Farrar JT, Abualnaja Y (2014b) Properties of Red Sea coastal currents. Cont Shelf Res 78:51–61. https://doi.org/10.1016/j.csr.2014.01.025

Clifford M, Horton C, Schmitz J, Kantha LH (1997) An oceanographic nowcast/forecast system for the Red Sea. J Geophys Res 102(25):101–25,122

Cochran JR, Martinez F (1988) Evidence from the northern Red Sea on the transition from continental to oceanic rifting. Tectonophysics 153:25–53

Cooper TF, De'ath G, Fabricius KE, Lough JM (2008) Declining coral calcification in massive Porites in two nearshore regions of the northern Great Barrier Reef. Glob Chang Biol 14:529–538

Davis KA, Lentz SJ, Pineda J, Farrar JT, Starczak VR, Churchill JH (2011) Observations on the thermal environment on Red Sea platform reefs: a heat budget analysis. Coral Reefs 30:25–36. https://doi.org/10.1007/s00338-011-0740-8

Davis SR, Pratt LJ, Jiang H (2015) The Tokar gap jet: regional circulation, diurnal variability, and moisture transport based on numerical simulations. J Clim 28:5885–5907

De Moel H, Ganssen G, Peeters F, Jung S, Kroon D, Brummer G, Zeebe R (2009) Planktonic foraminiferal shell thinning in the Arabian Sea due to anthropogenic ocean acidification. Biogeosciences 6:1917–1925

Defant A (1961) Physical oceanography, volume 2. Pergamon Press, Oxford, p 598

DeVantier L, Tourak E, Al-Shaikh K, De'ath G (2000) Coral communities of the central-northern Saudi Arabian Red Sea. Fauna of Arabia 18:23–66

Dore JE, Lukas R, Sadler DW, Church MJ, Karl DM (2009) Physical and biogeochemical modulation of ocean acidification in the central North Pacific. Proc Natl Acad Sci U S A 106:12235–12240

Dullo WC (2005) Coral growth and reef growth: a brief review. Facies 51:37–52

Dullo WC, Montaggioni L (1998) Modern Red Sea coral reefs: a review of their morphologies and zonation. In: Purser BH, Bosence DWJ (eds) Sedimentation and tectonics in rift basins Red Sea: Gulf of Aden. Springer, Dordrecht, pp 583–594

El-Asmar HM (1997) Quaternary isotope stratigraphy and paleoclimate of coral reef terraces, Gulf of Aqaba, South Sinai, Egypt. Quat Sci Rev 16:911–924

El-Shenawy MA, El-Samra ML (1996) Nitrogen fixation in the northern Red Sea. J. K.A.U Mar. Sci., 7, Special issue, Symposuim on Red Sea marine environment, pp 33–39

Eladawy A, Nadaoka K, Negm A, Abdel-Fattah S, Hanafy M, Shaltout M (2017) Characterization of the northern Red Sea's oceanic features with remote sensing data and outputs from a global circulation model. Oceanologia 59:213–237. https://doi.org/10.1016/j.oceano.2017.01.002

Eltaib EBA (2010) Tides analysis in the Red Sea in Port Sudan and Gizan. M.S. thesis, niversity of Bergen, Geophysical Institute, 61 pp

Emerson S, Hedges J (2008) Chemical oceanography and the marine carbon cycle. Cambridge University Press

Erez J, Reynaud S, Silverman J, Schneider K, Allemand D (2011) Coral calcification under ocean acidification and global change. In: Dubinsky Z, Stambler N (eds) Coral reefs: an ecosystem in transition. Springer, pp 151–176

Falkowski PG, Ziemann D, Kolber Z, Bienfang PK (1991) Role of eddy pumping in enhancing primary production in the ocean. Nature 352:55–58

Felis T, Pätzold J, Loya Y, Fine M, Nawar AH, Wefer G (2000) A coral oxygen isotope record from the northern Red Sea documenting NAO, ENSO, and North Pacific teleconnections on Middle East climate variability since the year 1750. Paleoceanography 15:679–694

Fricke HW, Knauer B (1986) Diversity and spatial pattern of coral communities in the Red Sea upper twilight zone (a quantitative assessment study by submersible). Oecologia 71:29–37

Fricke HW, Vareschi E, Schlichter D (1987) Photoecology of the coral *Leptoseris fragilis* in the Red Sea twilight zone (an experimental study by submersible). Oecologia 73:371–381

Gattuso JP, Frankignoulle M, Bourge I, Romaine S, Buddemeier RW (1998) Effect of calcium carbonate saturation of seawater on coral calcification. Glob Planet Chang 18:37–46

Genin A, Lazar B, Brenner S (1995) Vertical mixing and coral death in the Red Sea following the eruption of Mount Pinatubo. Nature 377:507–510

Grant WD, Madsen OS (1986) The continental-shelf bottom boundary-layer. Annu Rev Fluid Mech 18:265–305

Grant WD, Williams AJ, Glenn SM (1984) Bottom stress estimates and their prediction on the Northern California continental shelf during CODE-1. The importance of wave-current interaction. J Phys Oceanogr 14:506–527

Grasshoff K (1969) Zur Chemie des Roten Meeres und des Inneren Golfs von Aden nach Beobachtungen von FS "Meteor" während der Indischen Ozean Expedition 1964/65. Meteor Forschungsergebn, Reihe A, 6

Grover R, Ferrier-Pagès C, Maguer J-F, Ezzat L, Fine M (2014) Nitrogen fixation in the mucus of Red Sea corals. J Exp Biol 217:3962–3963. https://doi.org/10.1242/jeb.111591

Gvirtzman G (1994) Fluctuations of sea level during the past 400,000 years: the record of Sinai, Egypt (northern Red Sea). Coral Reefs 13:203–214

Gvirtzman G, Kronfeld J, Buchbinder B (1992) Dated coral reefs of southern Sinai (Red Sea) and their implication to late Quaternary Sea levels. Mar Geol 108:29–37

Harriott VJ, Fisk DA (1987) A comparison of settlement plate types for experiments on the recruitment of scleractinian corals. Mar Ecol Prog Ser 37:201–208

Hearn CJ (2010) Hydrodynamics of coral reefs. In: Hopley D (ed) Encyclopedia of modern coral reefs. Springer, Berlin, pp 563–573

Hench JL, Leichter JJ, Monismith SG (2008) Episodic circulation and exchange in a wave-driven coral reef and lagoon system. Limnol Oceanogr 53:2681–2694. https://doi.org/10.4319/lo.2008.53.6.2681

Hickey B, Goudie AS (2007) The use of TOMS and MODIS to identify dust storm source areas: the Tokar delta (Sudan) and the Seistan basin (South West Asia). In: Goudie AS, Kalvoda J (eds) Geomorphological variations. P3K, Prague, pp 37–57

Hoegh-Guldberg O, Mumby PJ, Hooten AJ, Steneck RS, Greenfield P, Gomez E, Harvell CD, Sale PF, Edwards AJ, Caldeira K, Knowlton N, Eakin CM, Iglesias-Prieto R, Muthiga N, Bradbury RH, Dubi A, Hatziolos ME (2007) Coral reefs under rapid climate change and ocean acidification. Science 318:1737–1742

Jarosz E, Murray SP, Inoue M (2005) Observations on the characteristics of tides in the Bab el Mandab Strait. J Geophys Res 110:C03015. https://doi.org/10.1029/2004JC002299.

Jiang H, Farrar JT, Beardsley RC, Chen R, Chen C (2009) Zonal surface wind jets across the Red Sea due to mountain gap forcing along both sides of the Red Sea. Geophys Res Lett 36:L19605

Joffe S, Garfunkel Z (1987) Plate kinematics of the circum Red Sea- a re-evaluation. Tectonophysics 141:5–22

Kalenderski S, Stenchikov G, Zhao C (2013) Modeling a typical wintertime dust event over the Arabian Peninsula and the Red Sea. Atmos Chem Phys 13:1999–2014

Kalenderski S, Stenchikov G (2016) High-resolution regional modeling of summertime transport and impact of African dust over the Red Sea and Arabian Peninsula. J Geophys Res Atmos 121:6435–6458. https://doi.org/10.1002/2015JD024480

Khalil SM, McClay KR (2009) Structural control on syn-rift sedimentation, northwestern Red Sea margin, Egypt. Mar Petrol Geol 26:1018–1034

Khimitsa VA, Bibik VA (1979) Seasonal exchange in dissolved oxygen and phosphate between the Red Sea and the Gulf of Aden. Oceanol 9:544–546

Kiflawi M, Belmaker J, Brokovich E, Einbinder S, Holzman R (2006) The determinants of species richness of a relatively young coral-reef ichthyofauna. J Biogeogr 33:1289–1294

Kleypas JA, McManus JW, Meñez LAB (1999) Environmental limits to coral reef development: where do we draw the line? Am Zool 39:146–159

Klinker J, Reiss Z, Kropach C, Levanon I, Harpaz H, Halicz E, Asaf G (1976) Observations on circulation pattern in Gulf of Elat (Aqaba), Red-Sea. Isr J Earth Sci 25:85–103

Krumgalz B, Erez J, Chen C (1990) Anthropogenic CO_2 penetration in the northern Red Sea and in the Gulf of Elat (Aqaba). Oceanol Acta 13:283–290

Kuffner IB, Andersson AJ, Jokiel PL, Rodgers KS, Mackenzie FT (2008) Decreased abundance of crustose coralline algae due to ocean acidification. Nat Geosci 1:114–117

Langodan S, Cavaleri L, Viswanadhapalli Y, Hoteit I (2014) The Red Sea: a natural laboratory for wind and wave modeling. J Phys Oceanogr 44:3139–3159

Langodan S, Viswanadhapalli Y, Dasari HP, Knio O, Hoteit I (2016) A high resolution assessment of wind and wave energy potentials in the Red Sea. Appl Energy 181:244–255

Langodan S, Cavaleri L, Viswanadhapalli Y, Pomaro A, Bertotti L, Hoteit I (2017a) The climatology of the Red Sea – part 1: the wind. Int J Climatol 37:4509–4517. https://doi.org/10.1002/joc.5103

Langodan S, Cavaleri L, Pomaro A, Viswanadhapalli Y, Bertotti L, Hoteit I (2017b) The climatology of the Red Sea - part 2: the waves. Int J Climatol 37:4518–4528. https://doi.org/10.1002/joc.5101

Lazar B, Erez J, Silverman J, Rivlin T, Rivlin A, Dray M, Meeder E, Iluz D (2008) Recent environmental changes in the chemical-biological oceanography of the Gulf of Aqaba (Eilat). In: Por FD (ed) Aqaba-Eilat, the improbable gulf. Environment, biodiversity and preservation. Magnes Press, Jerusalem

Legge H-L, Mutterlose J, Arz HW, Pätzold J (2008) Nannoplankton successions in the northern Red Sea during the last glaciation (60–14.5 ka BP): reactions to climate change. Earth Planet Sci Lett 270:271–279

Lentz SJ, Churchill JH, Davis KA, Farrar JT (2016a) Surface gravity wave transformation across a platform coral reef in the Red Sea. J Geophys Res Oceans 121:693–705. https://doi.org/10.1002/2015JC011142

Lentz SJ, Churchill JH, Davis KA, Farrar JT, Pineda J, Starczak V (2016b) The characteristics and dynamics of wave-driven flow across a platform coral reef in the Red Sea. J Geophys Res Oceans 121. https://doi.org/10.1002/2015JC011141

Lentz SJ, Davis KA, Churchill JH, DeCarlo TM (2017) Coral reef drag coefficients – water depth dependence. J Phys Oceanogr 47:1061–1075

Lowe RJ, Falter JL, Monismith SG, Atkinson MJ (2009) Wave-driven circulation of a coastal reef–lagoon system. J Phys Oceanogr 39(4):873–893. https://doi.org/10.1175/2008JPO3958.1

Luz B, Heller-Kallai L, Almogi-Labin A (1984) Carbonate mineralogy of Late Pleistocene sediments from the northern Red Sea. Isr J Earth-Sci 33:157–166

Lyne VD, Butman B, Grant WD (1990) Sediment movement along the U.S. east coast continental shelf—I. Estimates of bottom stress using the Grant-Madsen model and near-bottom wave and current measurements. Cont Shelf Res 10:397–428

Madah F, Mayerle R, Bruss G, Bento J (2015) Characteristics of tides in the Red Sea region, a numerical model study. Open J Mar Sci 5:193–209

Madsen OS, Wright LD, Boon JD, Chisholm TA (1993) Wind stress, bed roughness and sediment suspension on the inner shelf during an extreme storm event. Cont Shelf Res 13:1303–1324

Maillard C, Soliman G (1986) Hydrography of the Red Sea and exchanges with the Indian Ocean in summer. Oceanol Acta 9:249–269

Makovsky Y, Wunch A, Ariely R, Shaked Y, Rivlin A, Shemesh A, Avraham ZB, Agnon A (2008) Quaternary transform kinematics constrained by sequence stratigraphy and submerged coastline features: the Gulf of Aqaba. Earth Planet Sci Lett 271:109–122

Manasrah R, Hasanean HM, Al-Rousan S (2009) Spatial and seasonal variations of sea level in the Red Sea, 1958-2001. Ocean Sci J 44:145–159

Mass T, Kline DI, Roopin M, Veal CJ, Cohen S, Iluz D, Levy O (2010) The spectral quality of light is a key driver of photosynthesis and photoadaptation in *Stylophora pistillata* colonies from different depths in the Red Sea. J Exp Biol 213:4084–4091. https://doi.org/10.1242/jeb.039891

McDonald CB, Koseff JR, Monismith SG (2006) Effects of the depth to coral height ratio on drag coefficients for unidirectional flow over coral. Limnol Oceanogr 51(3):1294–1301

McGillicuddy DJ et al (2007) Eddy/wind interactions stimulate extraordinary mid-ocean plankton blooms. Science 316:1021–1026

Millero FJ, Lee K, Roche M (1998) Distribution of alkalinity in the surface waters of the major oceans. Mar Chem 60:111–130

Monismith SG (2007) Hydrodynamics of coral reefs. Annu Rev Fluid Mech 39:37–55. https://doi.org/10.1146/annurev.fluid.38.050304.092125

Monismith SG, Herdman LMM, Ahmerkamp S, Hench JL (2013) Wave transformation and wave-driven flow across a steep coral reef. J Phys Oceanogr 43:1356–1379

Montaggioni, L (2000) Postglacial reef growth. Comptes endus De L Academie Des Sciences Serie II Fascicule A-Sciences De La Terre Et Des Planetes, 331, 319–330

Montaggioni L (2005) History of indo-Pacific coral reef systems since the last glaciation: development patterns and controlling factors. Earth Sci Rev 71:1–75

Morcos SA (1970) Physical and chemical oceanography of the Red Sea. Oceanogr Mar Biol Annu Rev 8:73–202

Morse ANC, Iwao K, Baba M, Shimoike K, Hayashibara T, Omori M (1996) An ancient chemosensory mechanism brings new life to coral reefs. Biol Bull 191:149–154

Moy AD, Howard WR, Bray SG, Trull TW (2009) Reduced calcification in modern Southern Ocean planktonic foraminifera. Nat Geosci 2:276–280

Mucci A (1983) The solubility of calcite and aragonite in seawater at various salinities, temperatures and one atmosphere total pressure. Am J Sci 283:780–799

Murray SP, Johns W (1997) Direct observations of seasonal exchange through the Bab el Mandeb Strait. Geophys Res Lett 24:2557–2560

Naqvi SWA, Hansen HP, Kureishy TW (1986) Nutrient uptake and regeneration ratios in the Red Sea with reference to the nutrient budgets. Oceanol Acta 9:271–275

Neo ML, Todd PA, Teo SL-M, Chou LM (2009) Can artificial substrates enriched with crustose coralline algae enhance larval settlement and recruitment in the fluted giant clam (Tridacna squamosa)? Hydrobiologia 625:83–90

Neumann AC, McGill DA (1962) Circulation of the Red Sea in early summer. Deep-Sea Res 8:223–285

Orr JC, Fabry VJ, Aumont O, Bopp L, Doney SC, Feely RA, Gnanadesikan A, Gruber N, Ishida A, Joos F, Key RM, Lindsay K, Maier-Reimer E, Matear R, Monfray P, Mouchet A, Najjar RG, Plattner GK, Rodgers KB, Sabine CL, Sarmiento JL, Schlitzer R, Slater RD, Totterdell IJ, Weirig MF, Yamanaka Y, Yool A (2005) Anthropogenic Ocean acidification over the twenty-first century and its impact on calcifying organisms. Nature 437:681–686. https://doi.org/10.1038/nature04095

Oschlies A, Garçon V (1998) Eddy-induced enhancement of primary production in a model of the North Atlantic Ocean. Nature 394:266–269

Osipov S, Stenchikov G (2018) Simulating the regional impact of dust on the Middle East climate and the Red Sea. J Geophys Res Oceans 123:1023–1047. https://doi.org/. https://doi.org/10.1002/2017JC013335

Papadopoulos VP, Abualnaja Y, Josey SA, Bower A, Raitsos DE, Kontoyiannis H, Hoteit I (2013) Atmospheric forcing of the winter air-sea heat fluxes over the Northern Red Sea. J Clim 26:1685–1701

Papaud A, Poisson A (1986) Distribution of dissolved CO2 in the Red-Sea and correlations with other geochemical tracers. J Mar Res 44:385–402

Patzert WC (1974) Wind-induced reversal in Red Sea circulation. Deep-Sea Res 21:109–121

Phillips OM (1966) On turbulent convection currents and the circulation of the Red Sea. Deep Sea Res 13:1149–1160

Pierrot D, Lewis E, Wallace D (2006) CO2sys DOS program developed for CO2 system calculations. ORNL/CDIAC-105. Carbon dioxide information analysis center, oak Ridge National Laboratory. US Department of Energy, Oak Ridge

Pineda J, Starczak V, Tarrant A, Blythe J, Davis K, Farrar T, Beruman M, da Silva JCB (2013) Two spatial scales in a bleaching event: corals from the mildest and the most extreme thermal environments escape mortality. Limnol Oceanogr 58:1531–1545. https://doi.org/10.4319/lo.2013.58.5.153

Plahn O, Baschek B, Badewien TH, Walter M, Rhein M (2002) Importance of the Gulf of Aqaba for the formation of bottom water in the Red Sea. J Geophys Res Oceans 107:22-1–22-18

Poisson A, Morcos S, Souvermezoglou E, Papaud A, Ivanoff A (1984) Some aspects of biogeochemical cycles in the Red Sea with special references to new observations made in summer 1982. Deep-Sea Res 31:707–718

Prakash PJ, Stenchikov G, Kalenderski S, Osipov S, Bangalath H (2015) The impact of dust storms on the Arabian Peninsula and the Red Sea. Atmos Chem Phys 15:199–222

Prospero JM, Ginoux P, Torres O, Nicholson SE, Gill TE (2002) Environmental characterization of global sources of atmospheric soil dust identified with the Nimbus 7 Total Ozone Mapping Spectrometer (TOMS) absorbing aerosol product. Rev Geophys 40:2–1–2-31

Quadfasel D, Baunder H (1993) Gyre-scale circulation cells in the Red Sea. Oceanol Acta 16:221–229

Qurban MA, Balala AC, Kumar S, Bhavya PS, Wafar M (2014) Primary production in the Northern Red Sea. J Mar Syst 132:75–82

Raitsos DE, Hoteit I, Prihartato PK, Chronis T, Triantafyllou G, Abualnaja Y (2011) Abrupt warming of the Red Sea. Geophys Res Lett 38:L14601

Raitsos DE, Pradhan Y, Brewin RJW, Stenchikov G, Hoteit I (2013) Remote sensing the phytoplankton seasonal succession of the Red Sea. PLoS One 8:e64909. https://doi.org/10.1371/journal.pone.0064909

Ralston DK, Jiang H, Farrar JT (2013) Waves in the Red Sea: response to monsoonal and mountain gap winds. Cont Shelf Res 65:1–13

Roder C, Berumen ML, Bouwmeester J, Papathanassiou E, Al-Suwailem A, Voolstra CR (2013) First biological measurements of deep-sea corals from the Red Sea. Sci Rep. https://doi.org/10.1038/srep02802

Schlager W (2003) Benthic carbonate factories of the Phanerozoic. Int J Earth Sci 92:445–464

Shaked Y, Agnon A, Lazar B, Marco S, Avner U, Stein M (2004) Large earthquakes kill coral reefs at the north-west gulf of Aqaba. Terra Nova 16:133–138

Shaked Y, Lazar B, Marco S, Stein M, Tchernov D, Agnon A (2005) Evolution of fringing reefs: space and time constraints from the Guilf of Aqaba. Coral Reefs 24:165–172

Shanas PR, Aboobacker VM, Albarakati AMA, Zubier KM (2017a) Superimposed wind-waves in the Red Sea. Ocean Eng 138:9–22. https://doi.org/10.1016/j.oceaneng.2017.04.020

Shanas PR, Aboobacker VM, Albarakati AMA, Zubier KM (2017b) Climate driven variability of wind-waves in the Red Sea. Ocean Model 119:105–117. https://doi.org/10.1016/j.ocemod.2017.10.001

Siddall M, Rohling EJ, Almogi-Labin A, Hemleben C, Meischner D, Schmelzer I, Smeed DA (2003) Sea-level fluctuations during the last glacial cycle. Nature 423:853–858

Silverman J, Lazar B, Erez J (2007) Community metabolism of a coral reef exposed to naturally varying dissolved inorganic nutrient loads. Biogeochemistry 84:67–82

Silverman J, Lazar B, Cao L, Caldeira K, Erez J (2009) Coral reefs may start dissolving when atmospheric CO2 doubles. Geophys Res Lett 36:L05606–L05611

Silverman J, Lazar B, Erez J (2012) Carbon turnover rates in the one tree island reef: a 40-year perspective. Journal of geophysical research. Biogeosciences 117:G03023–G03039

Sofianos S, Johns W (2001) Wind induced sea level variability in the Red Sea. Geophys Res Lett 28:3175–3178

Sofianos SS, Johns WE (2002) An oceanic general circulation model (OGCM) investigation of the Red Sea circulation, 1. Exchange between the Red Sea and the Indian Ocean. J Geophys Res 107:3196. https://doi.org/10.1029/2001JC001184

Sofianos SS, Johns WE (2003) An oceanic general circulation model (OGCM) investigation of the Red Sea circulation: 2. Three dimensional circulation in the Red Sea. J Geophys Res 108(C3):3066. https://doi.org/10.1029/2001JC001185

Sofianos SS, Johns WE (2007) Observations of the summer Red Sea circulation. J Geophys Res 112:C06025. https://doi.org/10.1029/2006JC003886.

Sofianos SS, Johns WE, Murray SP (2002) Heat and freshwater budgets in the Red Sea from direct observations at Bab el Mandeb. Deep Sea Res Part II 49:1323–1340

Souvermezoglou E, Metzl N, Poisson A (1989) Red Sea budgets of salinity, nutrients, and carbon calculated in the strait of Bab-el-Mandab during the summer and winter season. J Mar Res 47:441–456

Stambler N (2005) Bio-optical properties of the northern Red Sea and the Gulf of Eilat Aqaba – Winter 1999. J Sea Res 54:186–203

Stambler N (2006) Light and picophytoplankton in the Gulf of Eilat (Aqaba). J Geophys Res 111:C11009

Steiner Z, Erez J, Shemesh A, Yam R, Katz A, Lazar B (2014) Basin-scale estimates of pelagic and coral reef calcification in the Red Sea and Western Indian Ocean. Proc Natl Acad Sci U S A 111:16303–16308

Sultan SAR, Ahmad F, Elghribi NM (1995a) Sea level variability in the Central Red Sea. Oceanol Acta 18(6):607–615

Sultan SAR, Ahmad F, El-Hassan A (1995b) Seasonal variations of the sea level in the central part of the Red Sea. Estuar Coast Shelf Sci 40:1–8

Sultan SAR, Ahmad F, Nassar D (1996) Relative contribution of external sources of mean sea-level variations at Port Sudan, Red Sea. Estuar Coast Shelf Sci 42:19–30

Symonds G, Black KP, Young IR (1995) Wave-driven flow over shallow reefs. J Geophys Res 100(C2):2639–2648. https://doi.org/10.1029/94JC02736

Talley LD (2013) Hydrographic Atlas of the World Ocean Circulation Experiment (WOCE): volume 4: Indian Ocean. International WOCE Project Office

Tragou E, Garrett C (1997) The shallow thermohaline circulation of the Red Sea. Deep-Sea Res Part I 44:1355–1376

Tragou E, Garrett C, Outerbridge R, Gilman G (1999) The heat and freshwater budgets of the Red Sea. J Phys Oceanogr 29:2504–2522

Triantafyllou G, Yao F, Petihakis G, Tsiaras KP, Raitsos DE, Hoteit I (2014) Exploring the Red Sea seasonal ecosystem functioning using a three-dimensional biophysical model. J Geophys Res Oceans 119:1791–1811. https://doi.org/10.1002/2013JC009641

Vercelli F (1925) Richerche di oceanografia fisica eseguite della R.N. AMMIRAGILIO MAGNAGHI (1923 – 24), part I, Correnti e maree. Ann Idrog 11:1–188

Vetter O, Becker JM, Merrifield MA, Pequignet A-C, Aucan J, Boc SJ, Pollock CE (2010) Wave setup over a Pacific Island fringing reef. J Geophys Res 115:C12066. https://doi.org/10.1029/2010JC006455

Viswanadhapalli Y, Dasari HP, Langodan S, Challa VS, Hoteit I (2017) Climatic features of the Red Sea from a regional assimilative model. Int J Climatol 37:2563–2581. https://doi.org/10.1002/joc.4865

Wahr J, Smeed DA, Leuliette E, Swenson S (2014) Seasonal variability of the Red Sea, from satellite gravity, radar altimetry, and in situ observations. J Geophys Res Oceans 119:5091–5104. https://doi.org/10.1002/2014JC010161

Weikert H (1987) Plankton and the pelagic environment. In: Edwards AJ, Head SM (eds) Key environments: Red Sea. Pergamon, Oxford, pp 90–111

Weiss R, Broecker W, Craig H, Spencer D (1983) Hydrographic data 1977–1978 GEOSECS Indian Ocean expedition, vol 5. National Science Foundation, Washington, DC

Winters G, Beer S, Zvi BB, Brickner I, Loya Y (2009) Spatial and temporal photoacclimation of *Stylophora pistillata*: zooxanthella size, pigmentation, location and clade. Mar Ecol Prog Ser 384:107–119

Wurgaft E, Steiner Z, Luz B, Lazar B (2016) Evidence for inorganic precipitation of CaCO3 on suspended solids in the open water of the Red Sea. Mar Chem 186:145–155

Yao F, Hoteit I, Pratt LJ, Bower AS, Zhai P, Kohl A, Gopalakrishnan G (2014a) Seasonal overturning circulation in the Red Sea: 1. Model

validation and summer circulation. J Geophys Res Oceans 119. https://doi.org/10.1002/2013JC009004

Yao F, Hoteit I, Pratt LJ, Bower AS, Kohl A, Gopalakrishnan G, Rivas D (2014b) Seasonal overturning circulation in the Red Sea: 2. Winter circulation. J Geophys Res Oceans 119. https://doi.org/10.1002/2013JC009331

Yehudai M, Lazar B, Bar N, Kiro Y, Agnon A, Shaked Y, Stein M (2017) U–Th dating of calcite corals from the Gulf of Aqaba. Geochim Cosmochim Acta 198:285–298. https://doi.org/10.1016/j.gca.2016.11.005

Zarokanellos ND, Kurten B, Churchill JH, Roder C, Voolstra CR, Abualnaja Y, Jones BH (2017a) Physical mechanisms routing nutri-

ents in the central Red Sea. J Geophys Res Oceans 122:9032–9046. https://doi.org/10.1002/2017JC013017

Zarokanellos ND, Papadopoulos VP, Sofianos SS, Jones BH (2017b) Physical and biological characteristics of the winter-summer transition in the central Red Sea. J Geophys Res Oceans 122:6355–6370. https://doi.org/10.1002/2017JC012882

Zhai P, Bower AS (2013) The response of the Red Sea to a strong wind jet near the Tokar gap in summer. J Geophys Res Oceans 118:422–434. https://doi.org/10.1029/2012JC008444

Zhan P, Subramanian AC, Yao F, Hoteit I (2014) Eddies in the Red Sea: a statistical and dynamical study. J Geophys Res Oceans 119:3909–3925. https://doi.org/10.1002/2013JC009563